



RESEARCH ARTICLE

Substrate interaction defects in histidyl-tRNA synthetase linked to dominant axonal peripheral neuropathy

Jamie A. Abbott¹ | Rebecca Meyer-Schuman² | Vincenzo Lupo³ | Shawna Feely⁴ |
 Inès Mademan^{5,6} | Stephanie N. Oprescu² | Laurie B. Griffin^{7,8} | M. Antonia Alberti⁹ |
 Carlos Casasnovas⁹ | Sharon Aharoni¹⁰ | Lina Basel-Vanagaite^{11,12,13,14} |
 Stephan Züchner¹⁵ | Peter De Jonghe^{5,6,16} | Jonathan Baets^{5,6,16} | Michael E. Shy⁴ |
 Carmen Espinós³ | Borries Demeler¹⁷ | Anthony Antonellis^{2,7}  |
 Christopher Francklyn¹ 

¹Department of Biochemistry, College of Medicine, University of Vermont, Burlington, Vermont

²Department of Human Genetics, University of Michigan Medical School, Ann Arbor, Michigan

³Unit of Genetics and Genomics of Neuromuscular Disorders, Centro de Investigación Príncipe Felipe (CIPF), Valencia, Spain

⁴Department of Neurology, University of Iowa Hospitals and Clinics, Iowa City, Iowa

⁵Neurogenetics Group, Center for Molecular Neurology, VIB, Antwerp, Belgium

⁶Laboratory of Neuromuscular Pathology, Institute Born-Bunge, University of Antwerp, Antwerpen, Belgium

⁷Cellular and Molecular Biology Program, University of Michigan Medical School, Ann Arbor, Michigan

⁸Medical Scientist Training Program, University of Michigan Medical School, Ann Arbor, Michigan

⁹Department of Neurology, Hospital Universitario de Bellvitge, Barcelona, Spain

¹⁰Institute of Child Neurology, Schneider Children's Medical Center of Israel, Sackler Faculty of Medicine, Tel Aviv University, Petah Tikva, Tel Aviv, Israel

¹¹Sackler Faculty of Medicine, Tel Aviv University, Tel Aviv, Israel

¹²Raphael Recanati Genetic Institute, Rabin Medical Center, Beilinson Campus, Petah Tikva, Israel

¹³Pediatric Genetics Unit, Schneider Children's Medical Center, Petah Tikva, Israel

¹⁴Felsenstein Medical Research Center, Rabin Medical Center, Petah Tikva, Israel

¹⁵Dr John T McDonald Foundation Department of Human Genetics & John P Hussman Institute for Human Genomics, University of Miami Miller School of Medicine, Miami, Florida

¹⁶Department of Neurology, Antwerp University Hospital, Antwerpen, Belgium

¹⁷Department of Biochemistry, The University of Texas Health Sciences at San Antonio, San Antonio, Texas

Correspondence

Anthony Antonellis, University of Michigan Medical School, 3710A Medical Sciences II, 1241 E. Catherine St. SPC 5618, Ann Arbor, MI.
 Email: antonell@umich.edu

Christopher Francklyn, University of Vermont, Health Sciences Complex, 89 Beaumont Ave. Burlington, VT.

Email: Christopher.Francklyn@uvm.edu

Funding information

Association Belge contre les Maladies Neuro-Musculaires, Grant/Award Number: 2012-305121 (NEUROMICS); National Institute of Neurological Disorders and Stroke, Grant/Award Numbers: NS065712, NS075764, NS092238; National Cancer Institute, Grant/Award Number: P30 CA054174; National Heart, Lung,

Abstract

Histidyl-tRNA synthetase (HARS) ligates histidine to cognate tRNA molecules, which is required for protein translation. Mutations in HARS cause the dominant axonal peripheral neuropathy Charcot-Marie-Tooth disease type 2W (CMT2W); however, the precise molecular mechanism remains undefined. Here, we investigated three HARS missense mutations associated with CMT2W (p.Tyr330Cys, p.Ser356Asn, and p.Val155Gly). The three mutations localize to the HARS catalytic domain and failed to complement deletion of the yeast ortholog (*HTS1*). Enzyme kinetics, differential scanning fluorimetry (DSF), and analytical ultracentrifugation (AUC) were employed to assess the effect of these substitutions on primary aminoacylation function and overall dimeric structure. Notably, the p.Tyr330Cys, p.Ser356Asn, and p.Val155Gly HARS substitutions all led to reduced aminoacylation, providing a direct connection between CMT2W-linked HARS mutations and loss of canonical ARS function. While DSF assays revealed that only one of the variants (p.Val155Gly) was less thermally stable relative to wild-type, all three HARS mutants formed stable dimers, as measured by AUC. Our work represents the first biochemical analysis of

and Blood Institute, Grant/Award Number: T32 HL007594-30; Research Fund-Flanders (FWO); National Institute of General Medical Sciences, Grant/Award Numbers: GM007315, GM007544, GM07863, GM118647, GM54899; Michigan Pre-doctoral Training in Genetics Program, Grant/Award Number: GM007544; Innovation by Science and Technology (IWT); National Institutes of Health Cellular and Molecular Biology Training Grant, Grant/Award Number: GM007315; National Institutes of Health F30 NRSA, Grant/Award Number: NS092238; Miguel Servet Program, Grant/Award Number: CPII14/00002; Muscular Dystrophy Association, Grant/Award Number: MDA294479; Aide à la Recherche ASBL; EU FP7/2007-2013, Grant/Award Number: 2012-305121; San Antonio Cancer Institute Grant

Communicated by Madhuri Hegde

CMT-associated *HARS* mutations and underscores how loss of the primary aminoacylation function can contribute to disease pathology.

KEYWORDS

aminoacyl-tRNA synthetase, Charcot-Marie-Tooth disease type 2W, hereditary motor and sensory neuropathy, histidyl-tRNA synthetase

1 | INTRODUCTION

With a prevalence of one in 2,500 individuals, Charcot-Marie-Tooth disease (CMT; also referred to as hereditary motor and sensory neuropathy) represents the most common inherited neuromuscular disorder. CMT disease is a heterogeneous group of peripheral neuropathies mainly characterized by muscle weakness and sensory loss in the distal extremities (Skre, 1974). Several subtypes of CMT have been described, including one form (CMT1) with primary Schwann cell pathology resulting in demyelination and decreased motor nerve conduction velocities (MNCVs), a second form (CMT2) with normal MNCVs but reduced amplitudes of muscle action potentials arising from axonal degeneration, and an intermediate form that has characteristics of both CMT1 and CMT2 (Dyck & Lambert, 1968; Pareyson & Marchesi, 2009a; Pareyson & Marchesi, 2009b; Pareyson, et al., 2009). CMT typically presents in an axon-length-dependent manner with the structures innervated by longer axons affected first. CMT specifically affects the extremities, causing progressive muscle weakening and wasting, decreased sensation, and skeletal deformities. The onset and penetrance of CMT is variable, with many patients experiencing symptoms in the first two decades of life. At the current time, there are no effective treatments for CMT.

Over 80 genes have been linked to CMT, distributed among diverse functional categories (Timmerman, Strickland, & Zuchner, 2014). Four genes account for the majority of CMT cases, consisting of peripheral myelin protein 22 (*PMP22*), myelin protein zero (*MPZ*), and gap junction beta-1 (*GJB1*), which are linked to CMT1, and mitofusin 2 (*MFN2*), which is linked to CMT2. In addition to myelin assembly, the diverse cellular processes affected by CMT include cytoskeleton/axonal transport, protein synthesis and quality control, endosomal sorting, mitochondrial function, channel abnormalities, and mRNA/processing transcription (Bird, 1993; Jerath & Shy, 2015). While the end result of CMT-associated mutations involves impaired Schwann cell or axon dysfunction, the precise mechanisms by which alterations of individual genes bring about these phenotypes is, for many genes, not well understood (Stum et al., 2011; Timmerman et al., 2014).

Among the genes linked to CMT are the aminoacyl-tRNA synthetases (ARSs), which attach amino acids to cognate tRNAs in the first step of translation (Antonellis & Green, 2008; Ibba & Soll, 2000). As essential protein synthesis factors, ARSs are present in all kingdoms and are ubiquitously expressed in all tissues. The human nuclear genome contains 37 ARS genes, of which 17 encode for a cytoplasmic synthetase, 17 encode for a mitochondrial synthetase, and three encode for bi-functional enzymes that charge tRNA in both cellular compartments. Interestingly, 31 ARS genes have been implicated in myriad dominant and recessive human disease phenotypes (Meyer-Schuman & Antonellis, 2017; Oprescu, et al., 2017). Many of the diseases linked to ARS mutations are severe, recessive developmental syndromes that affect multiple organs and tissues, including the central nervous system (Frohlich et al., 2017; Simons et al., 2015; Zhang et al., 2014). The majority of the disease-associated mutations have a clear loss-of-function effect, which is supported by the associated patient phenotype. For example, many ARS-associated recessive diseases are specific to mitochondrial ARS enzymes and lead to clear defects in the synthesis of electron transport chain protein synthesis and thus mitochondrial ATP output (Abbott, Francklyn, & Robey-Bond, 2014).

To date, five genes encoding a cytoplasmic or bi-functional ARS enzyme have been implicated in autosomal dominant CMT disease: glycyI-(*GARS*; MIM# 600287), tyrosyl-(*YARS*; MIM# 603623), alanyl-(*AARS*; MIM# 601065), histidyl-(*HARS*; MIM# 142810), and tryptophanyl-tRNA synthetase (*WARS*; MIM# 191050) (Jordanova et al., 2006; Latour et al., 2010; Safka Brozkova et al., 2015; Tsai et al., 2017; Vester et al., 2013). Methionyl-tRNA synthetase (*MARS*) variants have been identified in patients with peripheral neuropathy (Gonzalez et al., 2013; Hirano et al., 2016; Hyun et al., 2014; Nam et al., 2016). However, these variants were identified in single individuals or small families deeming the findings inconclusive. The first ARS implicated in CMT disease was *GARS*, where mutations were implicated in axonal CMT disease via positional cloning in families with an atypical disease presentation (Antonellis et al., 2003; Sivakumar et al., 2005). Notably, the majority of patients presented with an upper limb predominant

neuropathy that affected the intrinsic muscles of the hand (Antonellis et al., 2003; Sivakumar et al., 2005). Subsequently, *YARS*, *AARS*, *HARS*, and *WARS* mutations were identified in families with a more typical presentation of CMT disease (Jordanova et al., 2006; Latour et al., 2010; Safka Brozkova et al., 2015; Tsai et al., 2017; Vester et al., 2013).

HARS is unusual among the *ARS* in that different mutations in the gene encoding the cytoplasmic enzyme lead to two distinct inherited neurological syndromes. Initially, a single *HARS* mutation (P.Tyr454Ser) in the homozygous state was linked to recessive Usher Syndrome Type 3B in a small number of Amish children presenting with early onset loss of auditory and visual function (Puffenberger et al., 2012) (Abbott et al., 2017). Initial characterization of the mutant enzyme did not reveal a significant loss of aminoacylation, change in expression level, or change in intracellular localization. Subsequently, a candidate gene screen of 363 patients with CMT disease and no other previously acknowledged existing disease-causing alleles identified a *HARS* missense mutation (R137Q) in a single patient with peripheral neuropathy (Vester et al., 2013). More definitive evidence linking *HARS* mutations to CMT disease was provided by the identification of multi-generational pedigrees with inherited peripheral neuropathy that segregated with *HARS* missense mutations (T132I, P134H, D175E, and D364Y) (Safka Brozkova et al., 2015). While previous studies demonstrated consequences of *HARS* mutations consistent with pathogenicity, biochemical analyses on the primary function of *HARS* have yet to be performed.

Here, we report detailed biochemical analyses of *HARS* missense mutations identified in three families with autosomal dominant CMT disease. As part of our study, each mutant protein was expressed, purified, and characterized biochemically. The results indicate that each of the three mutations leads to a clear reduction in *HARS* catalytic activity. These findings provide the first indication that a substantial decrease in *HARS* catalytic activity is associated with CMT disease. The results are discussed in light of current models linking altered *ARS* activity to CMT pathophysiology.

2 | MATERIALS AND METHODS

2.1 | Clinical and genetic analysis of patients with peripheral neuropathy

2.1.1 | Family 1

We applied whole-exome sequencing to a cohort of index patients from 82 families with genetically undefined distal hereditary motor neuropathy for which mutations in the known pathogenic genes had previously been excluded. The Ethical Review Boards of the participating institutions approved this study. All patients or their legal representatives signed informed consent prior to enrolment. Blood sampling and DNA extraction was performed according to standard methods. The Nextera Rapid Capture Expanded Exome kit (62 Mb) (Illumina, San Diego, CA, USA) was used for exome enrichment. Subsequently, the libraries were sequenced on a HiSeq 2500 platform (Illumina, San Diego, CA, USA). The Burrows-Wheeler Aligner (BWA) tool was used

to perform the sequence alignment to the reference genome (hg19, UCSC Genome Browser). Variant calling was done with Genome Analysis Toolkit (GATK) Unified Genotyper. For the annotation and filtering, we used the Clinical Sequence Analyzer and Miner (Wuxi NextCODE). For further filtering of the data, following criteria were applied: no occurrence or a frequency $\leq 0.5\%$ of the variants in public exome variant repositories (Exome Aggregation Consortium, 1000 Genomes Project, Exome Variant Server, in-house data); variants with impact on the encoded protein (missense, nonsense, frame shift, inframe indels, and splice site variants); read depth ≥ 7 ; minimal heterozygous call percentage $\geq 20\%$, minimal homozygous call percentage $\geq 66\%$. In addition, all data were imported and re-annotated into the GENESIS (gem.app) platform, a Web-based tool for next generation sequencing data analysis (<https://thegenesisprojectfoundation.org/>) (Gonzalez et al., 2015). Patients were evaluated by means of details clinical examination in combination with nerve conduction studies according to standard methods.

2.1.2 | Family 2

All family members were studied at Bellvitte's University Hospital. Detailed neurological evaluation was performed on patients and unaffected subjects. Electrophysiological studies were performed using standard methods in all subjects. We classified the severity of neuropathy symptoms according to the CMT neuropathy score (CMTNS). Blood samples were obtained from all family members once informed consent had been given. Genomic DNA was extracted from peripheral blood leucocytes. *PMP22*, *MPZ*, *MFN*, and *GJB1* mutations were previously excluded in the index case. Subsequently, a CMT gene panel screen was employed to identify candidate disease-causing variants.

2.1.3 | Family 3

The family was evaluated in the University of Iowa CMT Clinic. Informed consent was obtained from all individuals and the study obtained the approval of the Institutional Review Board at the University of Iowa. Neurological examination and neurophysiological studies were performed. The second version of the CMTNS (CMTNSv2) and CMT Exam Score (CMTESv2) [1] were employed to evaluate neuropathy. The SureSelect Human All Exon 50 MB Kit (Agilent, Santa Clara, CA, USA) was used for in-solution enrichment, and the HiSeq 2500 instrument (Illumina) was used to produce 100 bp paired-end sequence reads. The BWA, Picard, and the GATK were used to align sequence reads and call variants. These data were imported into GENESIS (GEM.app) (Gonzalez et al., 2015) for further analysis and filtering of variants.

The following *HARS* variants were identified in each of the three families: c.464T > G; p.Val155Gly (Family 1); c.989A > G; p.Tyr330Cys (Family 2); and c.1067G > A; p.Ser356Asn (Family 3). *HARS* variant nomenclature for nucleotide and amino acid changes are based on accession numbers NM_002109.5 and NP_002100.2, respectively. The three *HARS* variants were submitted to ClinVar (<https://www.ncbi.nlm.nih.gov/clinvar/>) under the accession numbers SCV000611612 (p.Val155Gly), SCV000611613 (p.Tyr330Cys), and SCV000611614 (p.Ser356Asn).

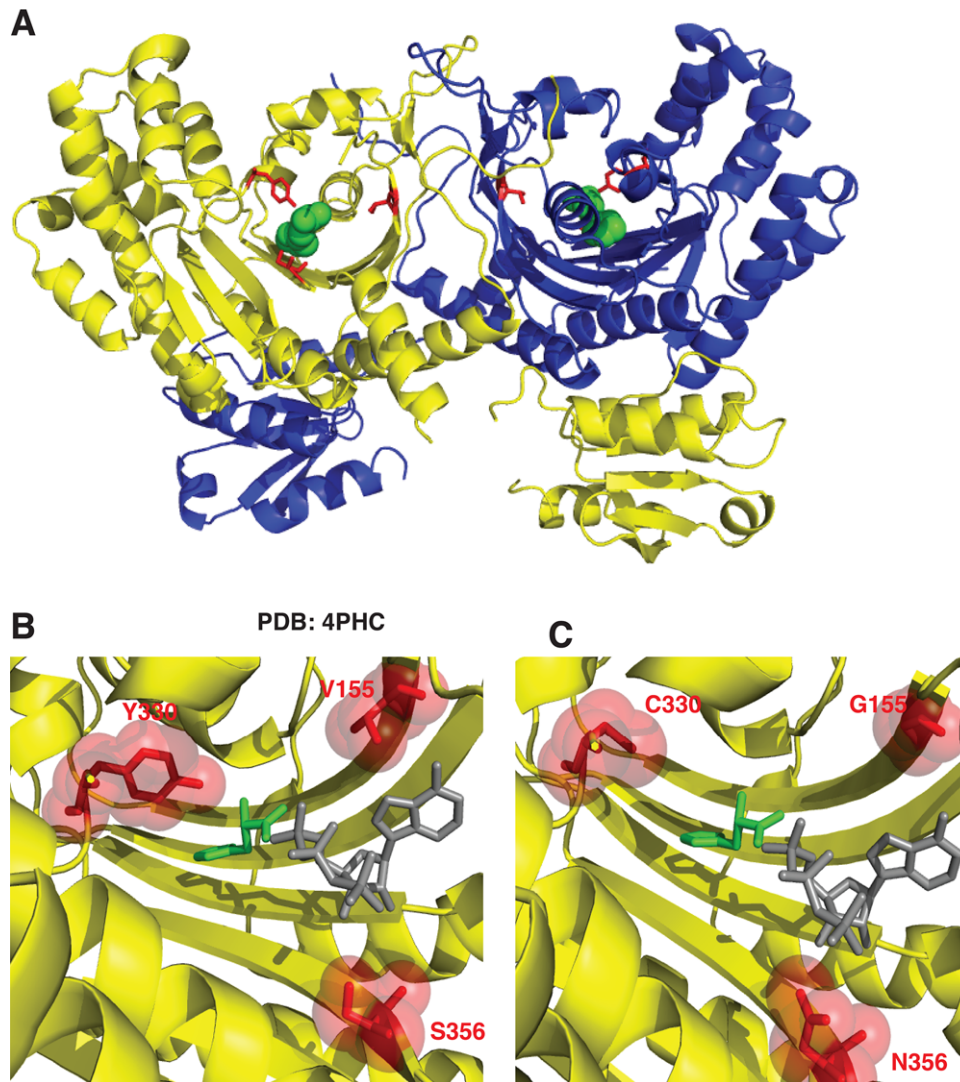


FIGURE 1 Histidyl-tRNA synthetase CMT variants are found in the active site of the dimeric enzyme. **A:** Histidyl-tRNA synthetase forms a homodimer (first monomer yellow and second monomer blue). The neuropathy-associated HARS residues are shown in the 3D structure as red sticks of the HARS dimer bound to histidine (green spheres) (PDB 4PHC). **B:** The HARS active site pocket (yellow) reveals that neuropathy-associated mutations face into the active site (shown as red sticks and spheres). **C:** Modeling in HARS neuropathy-associated substitutions indicates that interference with substrate binding (histidine green sticks and ATP gray sticks) can occur. ATP was modeled into the active site of the human HisRS bound to histidine (PDB 4PHC) by aligning the HisRS *E. coli* structure bound to ATP (PDB 1KMN)

2.2 | Computational assessment of HARS mutations

HARS protein sequences were collected from the NCBI Protein Database (<https://www.ncbi.nlm.nih.gov/protein/>) for the indicated species using the following accession numbers: human (*Homo sapiens*, NP_002100.2), mouse (*Mus musculus*, NP_032240.3), worm (*Caenorhabditis elegans*, NP_001023373.1), yeast (*Saccharomyces cerevisiae*, EDN61168.1), and bacteria (*Escherichia coli*, NP_289067.1). Multiple-species amino-acid sequence alignments were generated using Clustal Omega software (Larkin et al., 2007) and annotated with quaternary structural information by ENDscript (Robert & Gouet, 2014). Rendering of human HARS 3D protein structures and neuropathy-associated substitutions was performed by use of PYMOL using the coordinates corresponding to the structures of apo and histidine bound human cytosolic HARS (PDB IDs: 4PHC and 4 × 5O). The modeling of ATP into the active site of the human HARS-histidine com-

plex was performed by aligning this structure to the *E. coli* HARS-ATP complex (PDB 1KMN) using the Ce_align subroutine in PyMol. PyMol sessions of the aligned structures are available upon request. The PDB IDs used in this study include: 4PHC (Figure 1); 4 × 5O (Figure 2A); 4 × 5O and 1KMN; (Figure 2B); 4 × 5O and 1KMN (Figure 2C); 4 × 5O and 4PHC (Figure 2D); 4 × 5O (Figure 2E); and 4 × 5O and 1KMN (Figure 2F).

2.3 | Yeast complementation assays

Yeast complementation assays to study the functional consequences of HARS mutations were generated and performed as previously described (Vester et al., 2013). Each indicated missense variant was modeled in the yeast HARS ortholog *HTS1* or in the human HARS open-reading frame (primers available upon request). After

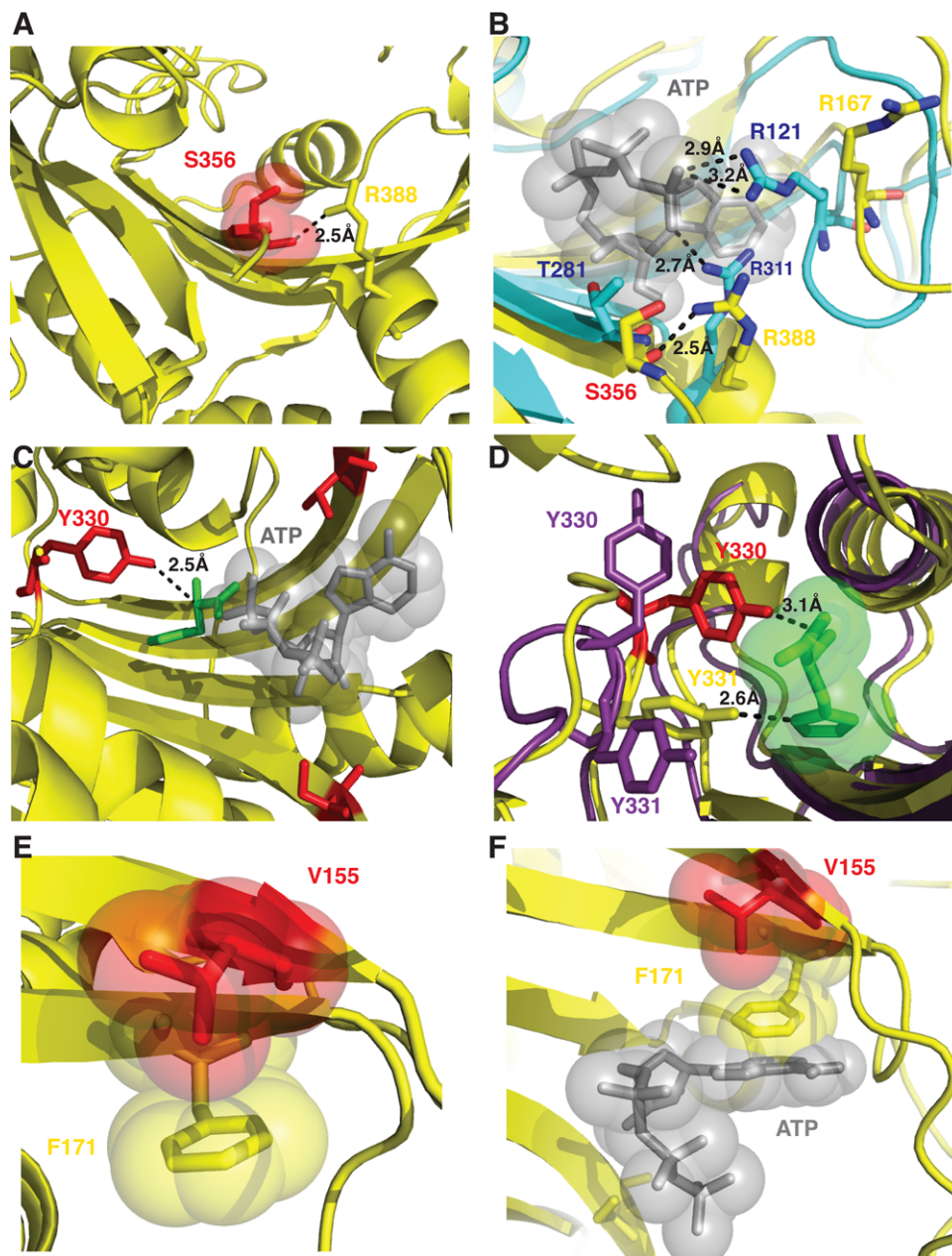


FIGURE 2 Molecular interactions of HARS neuropathy-associated amino-acid residues in the active site. **A:** S356 is positioned in the active site to coordinate a critical arginine residue R388 in motif 3. **B:** R388 is highly conserved and corresponds to R311 in *E. coli* HisRS structure (cyan) that is responsible for positioning the γ phosphate of ATP adjacent R121. **C:** Y330 is situated 2.5 Å from the alpha carbon of histidine (green) but makes no immediate interactions with modeled ATP (gray sticks and spheres). **D:** Y330 and Y331 facilitate hydrogen bonding interactions with histidine. Y330 in the apo enzyme (shown as purple sticks) can flip away from the active site and swing 8 Å upon histidine binding (shown as red sticks) to facilitate hydrogen bonding interactions. **E:** Phe 171 forms a stacking interaction with the ribose ring of ATP (as modeled in the active site as gray sticks and spheres). **F:** p.Val155Gly is buried in the active site and does not mediate any direct interactions with either substrate histidine or ATP, but in the apo enzyme forms a CH- π interaction with the aromatic ring of Phe 171 within the active site

mutagenesis, wild-type (WT) or mutant *HARS* or *HTS1* was cloned into pRS316 (Pierce et al., 2011), using the QuickChange II XL Site-Directed Mutagenesis Kit (Stratagene, San Diego, CA, USA). Resulting expression clones were purified and fully sequenced to confirm successful mutagenesis and rule out PCR-induced errors. A haploid Δ HTS1 strain (harboring a maintenance vector to express WT *HTS1* and *URA3*) was transformed with an empty vector ("Empty" in Figure 3A and B) or the appropriate WT or mutant *HTS1* or *HARS* in a *LEU2*-bearing vector and selected on medium lacking uracil and

leucine (Teknova). For each transformation, at least two independent plasmid preparations were used and at least two colonies from each plasmid were selected for additional analysis and grown to saturation for 2 days at 37°C in liquid media lacking uracil and leucine. A 10 μ l aliquot of each culture was spotted undiluted or diluted 1:10 or 1:100 in H₂O onto plates containing 0.1% 5-FOA (Teknova, Hollister, CA, USA) or medium lacking uracil and leucine and incubated at 30°C for 48–72 hr. Survival was determined by visual inspection of growth.

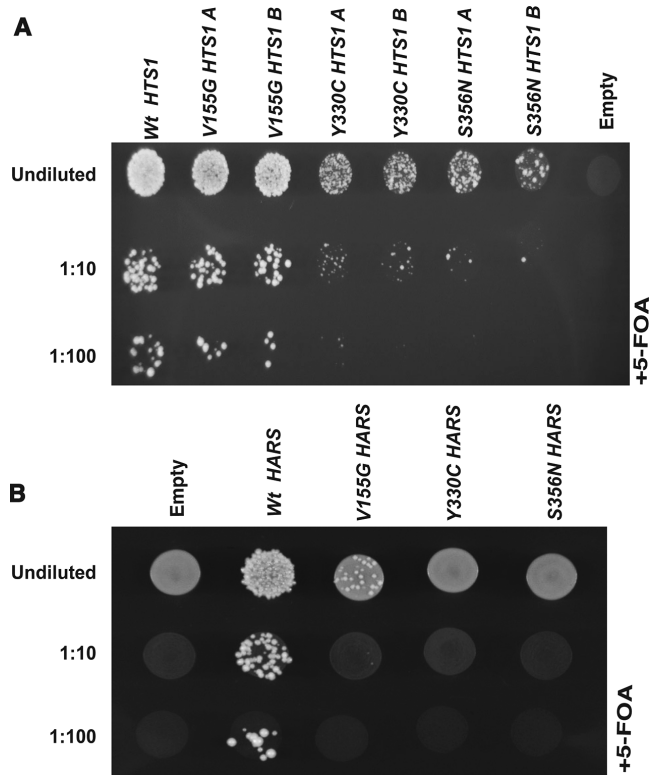


FIGURE 3 Neuropathy-associated *HARS* mutations result in loss-of-function in vivo. **A:** Yeast complementation analysis of *HARS* variants. Haploid Δ *HTS1* yeast strains were transformed with a vector containing no insert ("Empty") or an insert to express wild-type, p.Val155Gly, p.Tyr330Cys, or p.Ser356Asn *HTS1*. Two colonies (indicated by "A" and "B") from transformations with p.Val155Gly, p.Tyr330Cys, or p.Ser356Asn *HTS1* are shown. Resulting colonies (undiluted, diluted 1:10, or diluted 1:100) were grown on agar plates containing complete media with 0.1% 5-FOA. Note the severe depletion of growth associated with p.Tyr330Cys and p.Ser356Asn *HTS1* in the 1:10 and 1:100 dilutions. **B:** Similar yeast complementation assays as describe in A using the human *HARS* open-reading frame. Haploid Δ *HTS1* yeast strains were transformed with a vector containing no insert ("Empty") or an insert to express wild-type, p.Val155Gly, p.Tyr330Cys, or p.Ser356Asn *HARS*. After transformations, colonies (undiluted, diluted 1:10, or diluted 1:100) were grown on agar plates containing complete media with 0.1% 5-FOA. Note the severe depletion of growth associated with p.Val155Gly *HARS* in the undiluted sample and the lack of growth in the 1:10 and 1:100 dilutions

2.4 | Expression and purification of human *HARS* enzymes

Neuropathy-associated *HARS* mutations p.Ser356Asn, p.Tyr330Cys, and p.Val155Gly *HARS* containing plasmids were generated by QuickChange II Site-Directed Mutagenesis (Qiagen, Venlo, Netherlands) using the (pCAG/FLAG/RFC/A) plasmid with CAG promoter and FLAG-tag from GateWay vector Reading Frame Cassette A as a template (a generous gift from Dr. Robert Jinks) containing the gene for human WT N-terminal FLAG-tagged *HARS*. The following forward and reverse primers were used in the mutagenesis reactions for p.Ser356Asn, forward 5'-CCAGCAGCCACAT TGCC ACACCCAGG-3' and reverse 5'-CCTGGGTGTGGCAATGT GGCTGCTGG-3', for p.Tyr330Cys forward 5'-TCACCCAGTGTA

GCAATCCAGCCCTCGAG-3' and reverse 5'-CTCGAGGGCTGGATTG CTACTACTGGGGTGA-3' reverse, for p.Val155Gly 5-GGTTATCCCG CCGATATCC CTTTGCTATGTGGTAG-3' and reverse 5'-CTACCAC ATAGCAAAGGGATATCGG CGGGATAACC-3'. Successful mutagenesis of the *HARS* gene was analyzed by the Advanced Genome Technology Core sequencing facility at the University of Vermont and results were validated using Sequencher (Gene Codes Corporation, Ann Arbor, Michigan, USA). HEK293 cells were transiently transfected with plasmids expressing N-terminal FLAG-conjugated *HARS* gene for either WT or neuropathy-associated *HARS* mutants. Enzymes were purified by affinity and ion exchange chromatography as previously described (Abbott et al., 2017). Purified proteins were visualized by on a 10% SDS-PAGE gel.

2.5 | Multiple turnover aminoacylation kinetics

Multiple turnover aminoacylation assays were performed using a modified version of the Uhlenbeck-Wolfson assay as previously described (Abbott et al., 2017; Wolfson, Pleiss, & Uhlenbeck, 1998). Multiple turnover experiments were conducted in a buffer composed of (50 mM HEPES pH 7.5, 150 KCl, 10 mM MgCl₂, 5 mM β -ME, 2 U/ml PPIase and ³²P-labeled tRNA^{His}) at a fixed concentration of enzyme 5 nM for WT and (20 nM) for CMT variants with saturating concentrations of two of the three substrates. The saturating concentrations of tRNA^{His}, ATP, and histidine were 5 μ M, 10 mM, and 5 mM, respectively. The variable concentrations of these substrates were 100 nM to 15 μ M, 25 μ M to 5 mM, and 1 μ M to 5 mM, for tRNA^{His}, ATP and histidine, respectively. The concentration ranges tested for the mutant proteins typically employed a twofold to threefold higher final concentration for the variable substrate relative to the ranges employed for the WT protein. Initial rates were typically sampled over the first minute of the reaction. Reaction products were detected by radioisotopic imaging on a Phosphor Imaging screen (Bio-Rad Molecular Imager FXTM, Hercules, CA, USA). The concentration of aminoacylated tRNA^{His} was quantified by comparing the ratio of the relative amount of aminoacylated A76 (*aa*) (determined as counts \times mm²) to total radiolabeled product (*aa* + A76) according to Equation (1):

$$[AA - tRNA^{His}] = \frac{(AA_{counts} \times mm^2)}{(AA_{counts} \times mm^2) + (A76_{counts} \times mm^2)} \times [tRNA^{His}] \quad (1)$$

2.6 | Differential scanning fluorimetry

The differential scanning fluorimetry (DSF) experiments were carried out as previously described (Abbott et al., 2017). Briefly purified *HARS* proteins were incubated with 6 \times SYPRO orange dye and DSF buffer (25 mM HEPES pH 7.5, 50 mM KCl) at an enzyme concentration of 10 μ M in a 96-well microplate (Costar/Corning, Corning, NY, USA) to a final volume of 20 μ L. *T_m* values for apo enzymes were determined for two biological preparations of enzyme in triplicate for a final of six replicates. Enzymes were also incubated with either 10 mM histidine (*n* = 5), 5 mM ATP (*n* = 2), or 10 μ M tRNA^{His} for WT and 20 μ M tRNA^{His} (*n* = 3) for peripheral neuropathy-associated *HARS* mutations.

Scan rates were initiated at 26°C and heated at increments of 1°C per minute, to 95°C while fluorescence intensity was measured every 1°C. We fit the fluorescence data with GraphPad Prism 7 software as previously described (Abbott et al., 2017) to determine melting temperatures of HARS neuropathy-associated enzyme mutations and substrate complexes.

The melting temperature (T_m), defined as the midpoint of the protein unfolding transition curve, was determined using the Boltzman model as previously described (Niesen, Berglund, & Vedadi, 2007). GraphPad Prism 7 software was used to fit the fluorescence data (excluding data after maximal fluorescence intensity) to the Equation (2):

$$I = A + \frac{(B - A)}{1 + e^{(T_m - T)/C}} \quad (2)$$

2.7 | Analytical centrifugation sedimentation velocity experiments and analysis

Analytical centrifugation experiments were performed as previously described (Abbott et al., 2017). Briefly, purified enzymes (WT, p.Tyr330Cys, p.Val155Gly, and p.Ser356Asn) were dialyzed into a buffer containing 10 mM potassium phosphate buffer, 50 mM KCl, and no reducing agents. All protein samples were concentrated to 0.3 OD units/ml at 230 nm (0.7 μ M). Sedimentation velocity experiments were performed by the Center for Analytical Ultracentrifugation of Macromolecular Assemblies at the University of Texas Health Science Center at San Antonio, and conducted at 20°C, 35 K rpm, in a Beckman Optima XLI analytical ultracentrifuge using an An60Ti rotor and standard 2-channel epon centerpieces (Beckman-Coulter, Brea, CA, USA) and measured by UV intensity.

All data were examined with UltraScan-III ver. 3.5, release 2170 (Brookes E., 2006; Demeler et al., 2016) and hydrodynamic corrections for buffer density and viscosity was estimated to be 1.0019 g/ml and 0.998 cP, respectively. The partial specific volume of HARS (0.745 ml/g) was estimated by UltraScan from protein sequence analogous using methods outlined in Laue, Shah, Ridgeway, and Pelletier (1992). Experimental sedimentation data were pre-processed by two-dimensional spectrum analysis (Brookes, Cao, & Demeler, 2010; Demeler, 2010; Schuck, 1999) and fitted by the parametrically constrained spectrum analysis (PCSA), using a straight-line parameterization coupled with a Monte Carlo approach (Demeler, 2008; Gorbet et al., 2014). The calculations (Brookes, 2008) were performed on the Lonestar cluster at the Texas Advanced Computing Center at the University of Texas at Austin and on Comet and Gordon at San Diego Supercomputing Center.

3 | RESULTS

3.1 | Clinical and genetic analysis of patients with peripheral neuropathy

3.1.1 | Family 1

A three-generation family of Persian-Jewish descent (living in Israel) was identified with peripheral neuropathy (Figure 4A). Five affected

individuals are present and the family displays an autosomal dominant inheritance pattern with male-to-male transmission. The age of onset was in the second decade of life for the two youngest individuals, but the age of onset was less clear for the older individuals. In all cases, the affected status was clear upon examination. All individuals display a motor predominant to pure motor phenotype with clear pyramidal features as assessed by brisk reflexes and ankle clonus/Babinski signs. With one exception, all patients had normal sensory exams. At least two of the elder individuals have severe weakness necessitating the use of a cane or a wheelchair; however, the younger individuals are ambulatory. Nerve conduction studies are consistent with a motor predominant axonal neuropathy. There is some co-morbidity, as the female patient from the second generation has systemic lupus and one of the males in the third generation has uveitis, hematuria, and proteinuria.

Whole-exome sequencing was performed on one affected individual, which revealed common or non-segregating variants in *SLC5A7*, *SETX*, and *LAMA2* (the variant in *LAMA2* was not consistent with a dominant neuropathy). This analysis also revealed p.Val155Gly *HARS*, which fully segregated with the disease phenotype upon PCR and Sanger sequencing of additional individuals. Unfortunately, DNA was not available for the unaffected individual in the third generation. p.Val155Gly *HARS* affects an amino-acid residue found in the catalytic domain of the HARS enzyme (Figure 1A–C) and that is conserved from human to yeast (Figure 5). p.Val155Gly *HARS* has not been previously reported nor has it been detected in the gnomAD database (Table 1) (Lek et al., 2016).

3.1.2 | Family 2

A two-generation pedigree was identified with peripheral neuropathy (Figure 4B). The age of neuropathy onset for both patients was during childhood. Both individuals show a motor predominant phenotype, with distal motor deficit and atrophy, hammer toes, and pes cavus. Both affected patients have mild sensory symptoms in the toes, with reduced vibration sense at the knees. Tendon reflexes were brisk in both patients. The mother (patient 1) is restricted to a wheelchair while her son (patient 2) walks with difficulty but without aid. The CMTNS for patient 1 was 22 and 9 for patient 2. The phenotype of patient 1 is likely exacerbated by concomitant diseases (diabetes, chemotherapy for melanoma, radiculitis secondary to herpes zoster, and Parkinson's disease). Nerve conduction studies show axonal motor-predominant neuropathy in both patients.

Targeted gene panel screening in Family 2 (Figure 4B) revealed two missense *HARS* variants in cis: p.Ser227Ala and p.Tyr330Cys. These variants were previously reported as part of a larger study on CMT disease (Lupo et al., 2016) but the functional consequences of the mutations were not assessed. Both mutations segregate with the disease phenotype; however, p.Ser227Ala was deprioritized due to the number of alleles detected in gnomAD (37 alleles in 282,464 alleles total) and the lack of conservation of the affected residue (see Figure 5). p.Tyr330Cys *HARS* affects an amino-acid residue in the catalytic core of the HARS enzyme (Figure 1B) that is conserved from human to bacteria (Figure 5). p.Tyr330Cys has not been previously reported

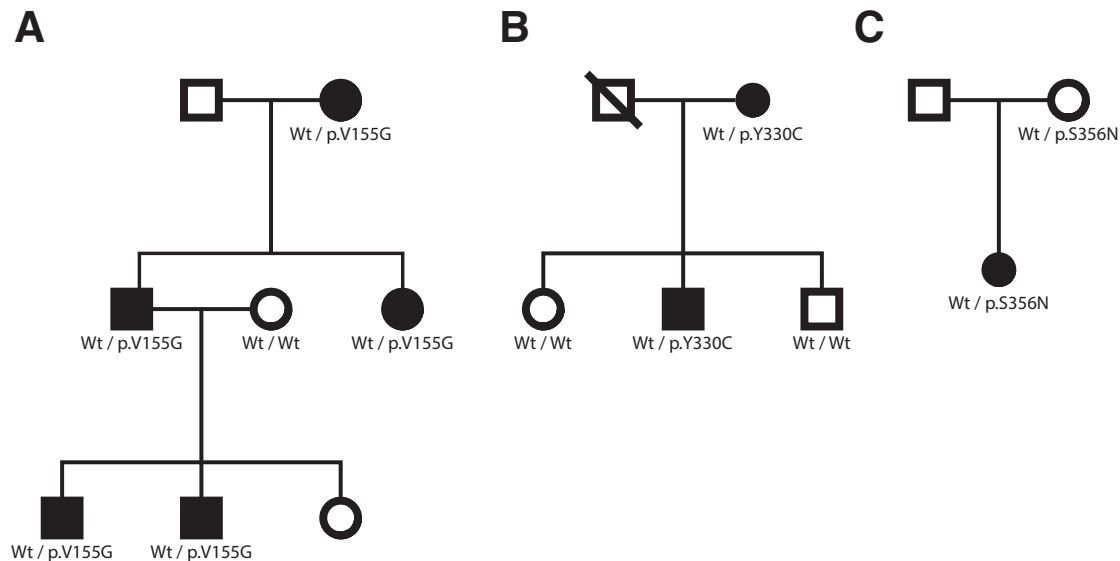


FIGURE 4 Histidyl-tRNA synthetase mutations identified in three pedigrees with peripheral neuropathy. **A–C:** Genotyping was performed to determine if *HARS* variants segregate with disease status. The pedigree structures of Family 1 (**A**), Family 2 (**B**), and Family 3 (**C**) are shown. Circles represent female individuals and squares represent male individuals. Shaded symbols represent affected individuals and non-shaded symbols represent unaffected individuals. Diagonal lines indicate deceased individuals. Genotypes are indicated under each individual where DNA was available

nor has it been detected in the gnomAD database (Table 1) (Lek et al., 2016).

3.1.3 | Family 3

A simplex pedigree was identified with two unaffected parents and a single daughter affected with peripheral neuropathy (Figure 4C). The affected daughter, at 15 years of age, was seen in consultation for difficulty with walking. Her early milestones were normal including walking with a normal gait at 12 months. She was physically active as a child and able to keep up with her peers until the age of 10 years. At 12 years of age, she noticed she could no longer walk on her heels. At ~13 years of age, she developed difficulties with walking. This progressed and she had problems with other activities such as jumping and running by the age of 15 years. She had ankle weakness, a foot drop, and right knee pain. She began to wear foot orthotics bilaterally. No problems with hand function were reported, but a slight hand tremor was reported and observed. Her sensory exam was normal to pinprick, light touch,

and joint position sense in all four extremities. Vibration sensation was also normal with the exception of a slight reduction at her toes. Her feet turned in bilaterally but could be brought to a neutral position. She had high arches and atrophy noted in her hands and distal forearms. Her CMTNS (Burns et al., 2012) was a 10, which is in the high end of the mild range. Her CMT Pediatric Score (Shy et al., 2005) was a 33, which is in the moderately impaired range.

Whole-exome sequencing was performed on the affected daughter in Family 3 (Figure 4C), which revealed p.Ser356Asn *HARS* as the only candidate disease-associated variant. Sanger sequencing revealed that this variant was inherited from the unaffected mother suggesting decreased penetrance or that this is a non-pathogenic variant. p.Ser356Asn *HARS* is also found in the active site of the *HARS* enzyme (Figure 1B and C) and that is conserved from human to yeast (Figure 5). p.Ser356Asn *HARS* has not been previously reported; however, it has been detected in the gnomAD database (five alleles in 277,222 chromosomes; Table 1) (Lek et al., 2016).

TABLE 1 *HARS* variants identified in patients with peripheral neuropathy

Amino-acid change ^a	Detection in gnomAD ^b	dbSNP accession no.	Position in yeast HTS1 ^c	Reference
p.Thr132Ile	Not detected	None	p.Thr131Ile	Safka Brozkova et al. (2015)
p.Pro134His	Not detected	None	p.Pro133His	Safka Brozkova et al. (2015)
p.Arg137Gln	20 / 246,154	rs191391414	p.Arg136Gln	Vester et al. (2013)
p.Val155Gly	Not detected	None	p.Val154Gly	This study
p.Asp175Glu	Not detected	None	p.Asp174Glu	Safka Brozkova et al. (2015)
p.Tyr330Cys	Not detected	None	p.Tyr330Cys	This study
p.Ser356Asn	5 / 277,222	rs144322728	p.Ser370Asn	This study
p.Asp364Tyr	Not detected	None	p.Asp378Tyr	Safka Brozkova et al. (2015)

^aHuman amino-acid positions are relative to GenBank Accession number NP_002100.2.

^b<https://gnomad.broadinstitute.org>.

^cYeast amino-acid coordinates correspond to GenBank accession number EDN61168.1.

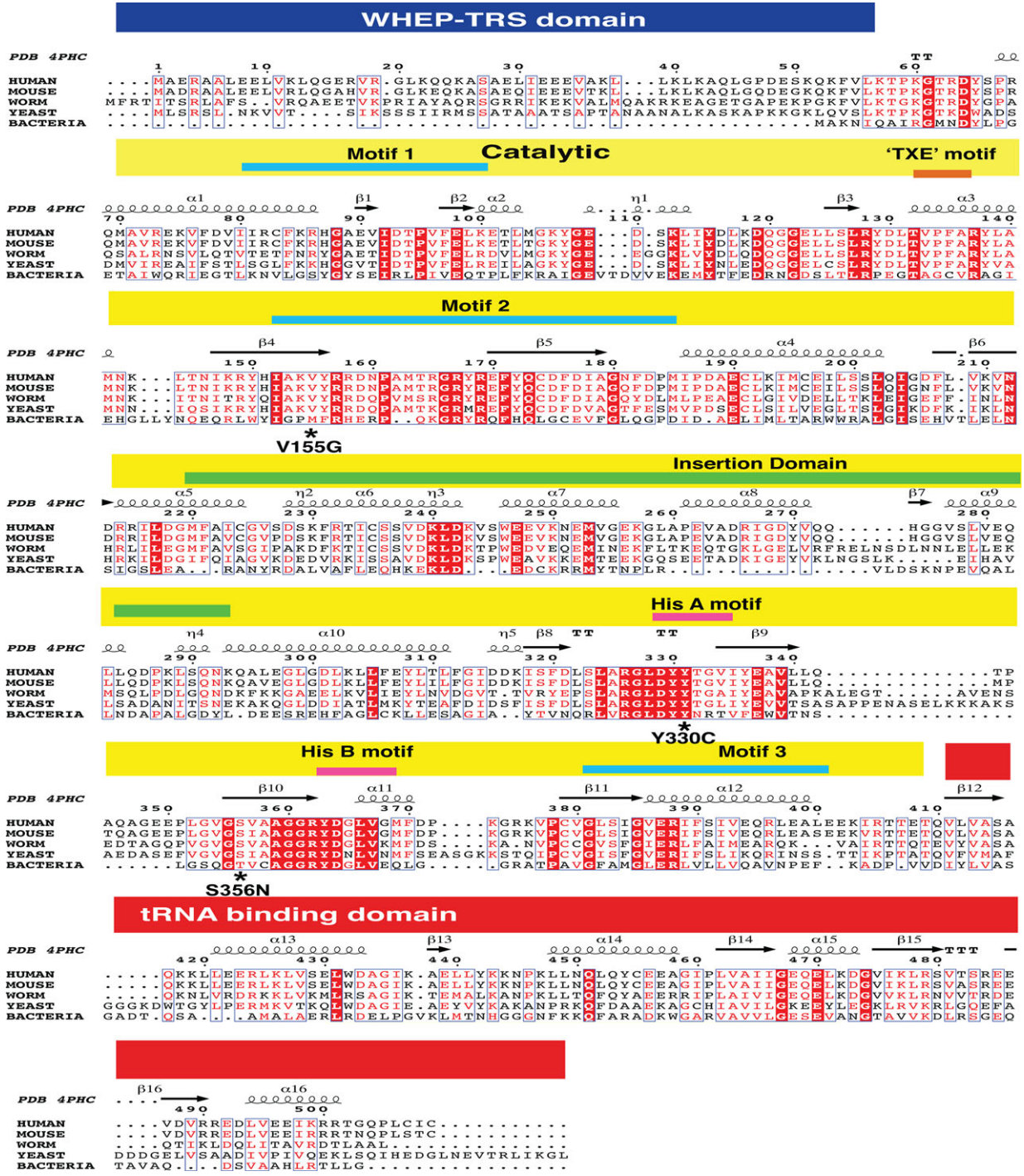


FIGURE 5 Neuropathy-associated HARS mutations are highly conserved. **A:** Multiple-species protein alignments were generated to assess the conservation of each affected amino-acid position. Complete amino-acid sequence alignment of human, mouse, worm, yeast, and bacterial HARS were generated with Clustal Omega and annotated with quaternary structural information with ENDscript (Robert & Gouet, 2014). The position of known functional domains of the HARS protein indicated in blue (WHEP-TRS domain of unknown function), red (catalytic core), and yellow (tRNA binding domain) and motifs critical for substrate binding are indicated along the top. For each of the three variants, the affected amino acid is indicated by an * in the HARS protein sequence in multiple, evolutionarily diverse species. Note that strictly conserved residues are highlighted in red with white lettering while slightly conserved residues across multiple but not all species are red

3.2 | The identified HARS mutations affect viability in yeast complementation studies

To test the functional consequences of the HARS missense variants described above (p.Val155Gly, p.Tyr330Cys, and p.Ser356Asn), each

variant was introduced into the yeast ortholog *HTS1* to model the effect of the mutation in the context of a eukaryotic cell (Table 1). Yeast complementation assays were then performed to independently test each missense change for the ability to support yeast cell growth compared with WT *HTS1* or an empty vector. A haploid yeast strain

(with the endogenous *HTS1* locus deleted and a maintenance vector to express WT *HTS1* and *URA3*) was transformed with either a pRS315 vector with no insert ("Empty"), a pRS315 vector harboring WT *HTS1*, or a mutant version encoding one of the three missense mutations (p.Val155Gly, p.Tyr330Cys, or p.Ser356Asn). Yeast cells were then selected on media containing 5-FOA, which is toxic to yeast carrying the *URA3*-bearing maintenance vector (Boeke, LaCroute, & Fink, 1984). Thus, only yeast cells expressing a functional *HTS1* allele from the pRS315 vector will grow in this assay.

Yeast transformed with a WT *HTS1* expression vector demonstrated significant growth, while those transformed with an empty vector did not (Figure 3A), consistent with *HTS1* being an essential gene (Vester et al., 2013). Yeast expressing p.Tyr330Cys or p.Ser356Asn *HTS1* displayed severely depleted, but not ablated, yeast cell growth (Figure 3A), indicating that these are hypomorphic alleles. In contrast, p.Val155Gly *HTS1* supported yeast cell growth in a manner similar to WT *HTS1* (Figure 3A). Growth at 37°C did not affect the cellular phenotype associated with the above mutations (data not shown). In summary, our previously employed *in vivo* yeast complementation assay demonstrated that p.Val155Gly *HTS1* supports growth similar to WT *HTS1*, and that S365N and p.Tyr330Cys *HTS1* are hypomorphic alleles in this assay.

The lack of a cellular growth defect associated with p.Val155Gly *HTS1* was surprising given that this mutation segregates with disease in a three-generation family. One possible explanation for this discrepancy may be differential effects of p.Val155Gly on the function of yeast *HTS1* compared with human *HARS*. To explore this possibility, we attempted to rescue deletion of yeast *HTS1* with the full-length human *HARS* protein. In yeast complementation assays similar to those described above, expressing human *HARS* rescued yeast cell growth while a vector with no *HARS* insert did not (Figure 3B). This confirms a similar finding that was recently reported (Lee et al., 2017). We next mutated the *HARS* expression construct to harbor the three missense mutations (p.Val155Gly, p.Tyr330Cys, or p.Ser356Asn) and found that p.Tyr330Cys and p.Ser356Asn *HARS* did not support any yeast cell growth indicating that they are functional null alleles (Figure 3B). Interestingly, p.Val155Gly *HARS* supported growth, but in a manner that is severely reduced compared to WT *HARS* (Figure 3B). These data indicate that p.Val155Gly *HARS* is a hypomorphic allele. Combined, our *in vivo* functional analyses indicate that p.Val155Gly, p.Tyr330Cys, and p.Ser356Asn *HARS* are loss-of-function alleles.

3.3 | Multiple-turnover kinetics identify specific catalytic deficiencies of HARS mutations

The results of the yeast complementation assays and the location of these neuropathy-associated *HARS* mutations in the catalytic domain raised the possibility that these substitutions compromise catalytic function. As an initial characterization of catalytic function, the production of histidyl-tRNA by each mutant and a WT control was monitored over a ten-minute time course in the presence of saturating concentrations of all three cognate substrates. In excellent agreement with the yeast complementation results, the two non-complementing mutants (p.Ser356Asn and p.Tyr330Cys *HARS*) generated about 20%

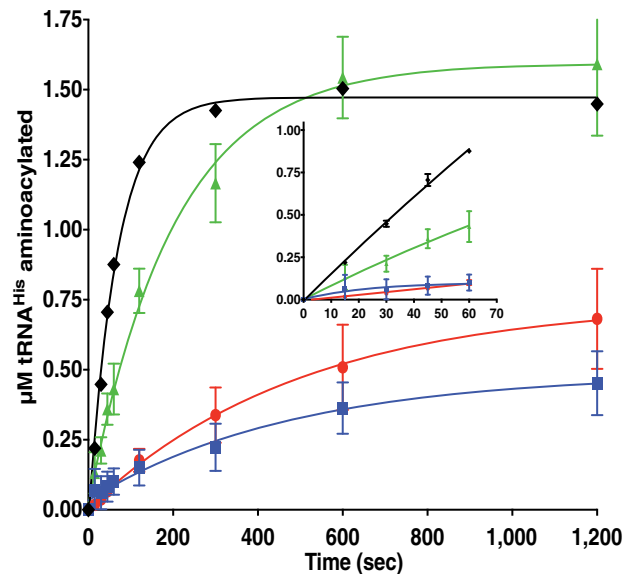


FIGURE 6 Neuropathy-associated HARS mutations reduce aminoacylation function. Progress curves for aminoacylation of tRNA^{His} substrates with histidine by wild-type or mutant HARS enzymes under conditions of excess substrates and limiting enzyme. Reaction conditions utilized saturating substrates (10 mM ATP, 10 mM histidine, and 10 μM tRNA^{His}) with either wild-type or mutant HARS enzymes. The progress of the reaction was followed by detection of aminoacylated ³²P radiolabeled over time, as described in *Materials and Methods*. The progress curves are color coded as follows: wild-type HARS (black diamonds, ◆); p.Val155Gly HARS (green triangles, ▲); p.Tyr330Cys HARS (red circles, ●), and p.Ser356Asn HARS (blue squares, ■). Each point represents the mean of three independent experiments, and error bars indicate the standard error. Inset, progress curves over the first 60 sec

of the amount of charged tRNA^{His} generated by WT and p.Val155Gly HARS in 10 min (Figure 6). Despite its near WT level of product accumulation after 10 min, the initial rate of product formation by the p.Val155Gly mutant was approximately 50% of the WT protein, indicating that this mutant is at least partially compromised for aminoacylation (Figure 6, inset).

In order to assess the effect of the mutant substitutions on the recognition of individual substrates, the ³²P-tRNA aminoacylation experiments were repeated under multiple turnover conditions employing fixed nanomolar concentrations of enzyme and varying substrate concentrations. In the first set of kinetic experiments, aminoacylation was monitored in presence of varying concentrations of tRNA and saturating concentrations of histidine and ATP. This set of experiments showed that, while none of the mutants exhibited an elevated K_M for tRNA^{His}, p.Tyr330Cys and p.Ser356Asn HARS exhibited nine-fold and 18-fold reductions (0.6 sec⁻¹ and 0.3 sec⁻¹, vs. 5.4 sec⁻¹ for WT) in the steady-state k_{cat} for aminoacylation, relative to WT HARS (Figure 7 and Table 2). By comparison, the p.Val155Gly HARS mutant exhibited a modest two-fold reduction in k_{cat} (Figure 7 and Table 2). These results confirm and extend the previous yeast complementation and product formation assays.

When histidine was the variable substrate and tRNA and ATP were the fixed concentration substrates, the turnover numbers for each of the mutants were similar to the values obtained in experiments

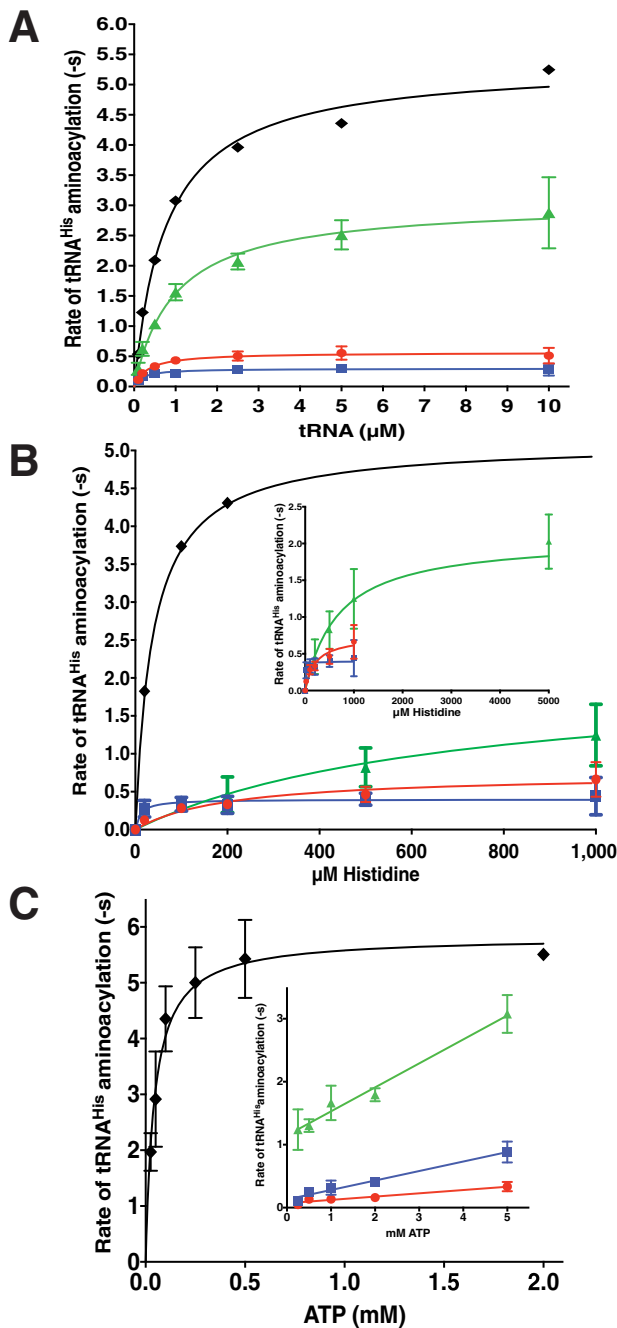


FIGURE 7 Identification of specific catalytic defects in neuropathy-associated HARS CMT mutants by steady-state kinetics. Multiple turnover aminoacylation reactions were performed under Michaelis-Menten conditions of excess substrates and limiting enzyme as described in *Materials and Methods*. Initial velocity of product formation was plotted against substrate concentration for **A**, tRNA; **B**, histidine, and **C**, ATP. Fits to the Michaelis-Menten equation returned k_{cat} and K_M values, which are reported in Table 2. The plots are color coded as in Figure 6: wild-type HARS (black diamonds, \blacklozenge); p.Val155Gly HARS (green triangles, \blacklozenge); p.Tyr330Cys HARS (red circles, \bullet), and p.Ser356Asn HARS (blue squares, \blacksquare). When ATP was the variable substrate, none of the mutants reached a saturating velocity at the highest ATP concentration (5 mM). The inset shows linear fits of the V/S data for the mutants to allow an estimation of k_{cat}/K_M . Each point represents the mean of three independent experiments, and error bars indicate the standard error

where tRNA was the variable substrate (Figure 7 and Table 2). The most significant kinetic differences were seen with the p.Tyr330Cys and p.Val155Gly HARS mutants. The K_M for histidine was elevated 25-fold for p.Tyr330Cys HARS, and at least 86-fold for p.Val155Gly HARS (Figure 7 and Table 2). These results illustrate that, despite the fact that p.Tyr330Cys and p.Val155Gly HARS both exhibit deficits in histidine binding, the activity of the p.Val155Gly HARS mutant alone can be rescued by elevated concentrations of histidine. Additionally, these results suggest that the diminished k_{cat} associated with p.Ser356Asn HARS appears not be linked to a decrease in binding to histidine.

The final set of steady-state kinetic experiments investigated the kinetics of aminoacylation under conditions of variable ATP concentrations and saturating histidine (10 mM) and tRNA^{His} (5 μ M). Kinetic experiments for the WT enzyme indicate that, under these substrate conditions, the K_M value for ATP in the aminoacylation reaction is 44.2 μ M (Table 2). This is comparable to the value of 140 μ M determined for the *S. typhimurium* WT HisRS catalyzed aminoacylation reaction (De Lorenzo, Straus, & Ames, 1972). Initial pilot experiments conducted with the mutants indicated that substantially higher titration ranges had to be employed in order to accurately determine parameters. Even under these conditions, saturating velocities were not obtained with any of the mutants. However, plotting the velocities against the concentration of [ATP] yielded straight lines from which estimates of the second order rate constant V/K_M could be obtained (Figure 7C). Relative to WT HARS, all three mutants showed significant decreases in V/K_M for ATP, corresponding to 342-fold for p.Val155Gly HARS, 866-fold for p.Ser356Asn HARS, and 2,549-fold for p.Tyr330Cys HARS (Table 2). Based on these results, we conclude that, for all three mutants, a major component of the attenuated catalytic activity originates from a significant increase in K_M for ATP. It is noteworthy that, while we were unable to achieve saturation at 5 mM ATP, we were able to reproduce k_{cat} results with 10 mM ATP in both the tRNA and histidine titrations (Table 2). In summary, we conclude that the HARS neuropathy-associated mutations lead to significant decreases in catalytic activity, typically reflected in decreases in k_{cat} and increases in the K_M for ATP binding.

3.4 | DSF reveals one out of three HARS mutations is unstable and two mutations have substrate binding defects

DSF is a useful technique that can be used to assess the melting temperature stabilizing effect of a substrate with respect to an enzyme, as well as aid in the evaluation of the effect of a potential pathogenic missense variant on protein structure (Abbott et al., 2017). Previously, incubation of HARS with saturating concentrations of the histidine amino-acid ligand raised the thermal shift transition temperature by seven degrees (Abbott et al., 2017). On the basis of the kinetic results indicating weaker binding of both histidine and ATP, we predicted that one or more the mutants would show altered thermal shift behavior. Thermal shift assays were performed for each combination of mutant enzyme and substrate. Consistent with the previous

TABLE 2 Steady-state kinetics of tRNA^{His} aminoacylation by human and neuropathy-associated mutations of histidyl-tRNA synthetases

	variable substrate			Histidine			ATP			References
	tRNA			K_M (μM)	k_{cat} (sec^{-1})	k_{cat}/K_M ($\mu\text{M}^{-1}\text{sec}^{-1}$)	K_M (μM)	k_{cat} (sec^{-1})	k_{cat}/K_M ($\mu\text{M}^{-1}\text{sec}^{-1}$)	
WT HARS	0.782 ± 0.101	5.4 ± 0.2	6.9	8.0 ± 4.0	4.1 ± 0.4	0.5 ± 0.4	44.2 ± 5.5	5.8 ± 0.2	0.13	ATP data this work
p.Ser356AsnHARS	0.199 ± 0.059	0.30 ± 0.02	1.5	10.8 ± 9.1	0.39 ± 0.04	0.04	ND	ND	$1.5 \times 10^{-4} \pm 1.2 \times 10^{-5}$	This work
p.Tyr330CysHARS	0.330 ± 0.072	0.56 ± 0.03	1.7	202.9 ± 83.23	0.74 ± 0.10	0.004	1.763 ± 544	0.48	0.000272	This work
p.Val155GlyHARS	0.979 ± 0.159	3.05 ± 0.14	3.1	687.2 ± 200.0	2.08 ± 0.16	0.003	ND	ND	$3.8 \times 10^{-4} \pm 2.7 \times 10^{-5}$	This work
<i>E. coli</i> HisRS	0.34 ± 0.05	1.71 ± 0.06	5.0	35.4 ± 3.7 ^a	133 ± 2.2 ^a	3.8 ^a	380	ND	ND	Fahoum and Yang (1987)

Values reported are the mean ± standard error of three independent experiments.

^aData are for histidine in the pyrophosphate exchange reaction.

TABLE 3 Thermal stability of neuropathy-associated HARS variants and substrate complexes

Enzyme	T_m ($^{\circ}\text{C}$)	ΔT_m ($^{\circ}\text{C}$) ^a	ΔT_m ($^{\circ}\text{C}$) ^b
WT	51.72 ± 0.44***	-	-
WT + histidine	58.75 ± 0.41	7.03	-
WT + ATP	53.76 ± 0.21	2.04	-
WT + tRNA ^{His}	53.43 ± 0.41	1.71	-
p.Ser356Asn	50.87 ± 0.33	-	-0.85
p.Ser356Asn + histidine	59.17 ± 0.31	8.30	0.42
p.Ser356Asn + ATP	53.12 ± 0.11	2.25	0.64
p.Ser356Asn + tRNA ^{His}	55.16 ± 0.20	4.29	NA
p.Tyr330Cys	51.72 ± 0.36	-	0
p.Tyr330Cys + histidine	55.95 ± 0.32	4.23	-2.8
p.Tyr330Cys + ATP	53.85 ± 0.12	2.13	0.09
p.Tyr330Cys + tRNA ^{His}	55.88 ± 0.29	4.16	NA
p.Val155Gly	48.05 ± 0.39***	-	-3.67
p.Val155Gly + histidine	49.35 ± 0.67	1.30	-9.4
p.Val155Gly + ATP	51.09 ± 0.16	3.04	-2.67
p.Val155Gly + tRNA ^{His}	53.91 ± 0.26	5.86	NA

Bold values were previously determined (Abbott et al., 2017).

Values reported are the mean ± standard error of two independent experiments in triplicate. Values that are significantly different WT to Val155Gly are indicated as *** $P < 0.0001$ (extra sum-of-squares F test).

^aRelative to the apo form of the same enzyme.

^bRelative to the same form of WT HARS enzyme.

kinetic data, there was an inverse relationship between the K_M for histidine of a given mutant protein and the extent of temperature stability provided by incubation with histidine in the assay. As seen in Figure 8 and Table 3, p.Ser356Asn HARS exhibited the same extent of stabilization by histidine (8.3° vs. 7.03°) as WT HARS, consistent with its essentially equivalent K_M in aminoacylation. By contrast, p.Tyr330Cys HARS and p.Val155Gly HARS exhibited smaller histidine-mediated temperature shifts (4.2° and 1.3°, respectively) consistent with their substantially increased Michaelis constants for histidine (202.9 and 687.2 μM fold, respectively).

For WT HARS, the ATP and tRNA-mediated temperature shifts are much smaller (2.04° and 1.7°, respectively) than that provided by histidine (Figure 8 and Table 3). In the presence of saturating ATP (5 mM), all three neuropathy-associated mutations had slightly increased ΔT_m values, corresponding to least 2°C for p.Tyr330Cys and p.Ser356Asn, and 3°C for p.Val155Gly (Table 3). In the presence of 20 μM tRNA^{His}, all three mutants exhibited 1°C in ΔT_m increases in stability (Table 3). Notably, none of the three mutants showed a significantly altered melting temperature in the presence of either ATP or tRNA, despite the fact that all three show substantially reduced apparent second order rate constants associated with ATP binding (Table 3).

3.5 | Analytical ultracentrifugation confirms that HARS neuropathy-associated mutations do not disrupt enzyme dimerization

Previous studies investigating mutations in the GARS gene linked to CMT have reported that a subset of the mutant substitutions lead to

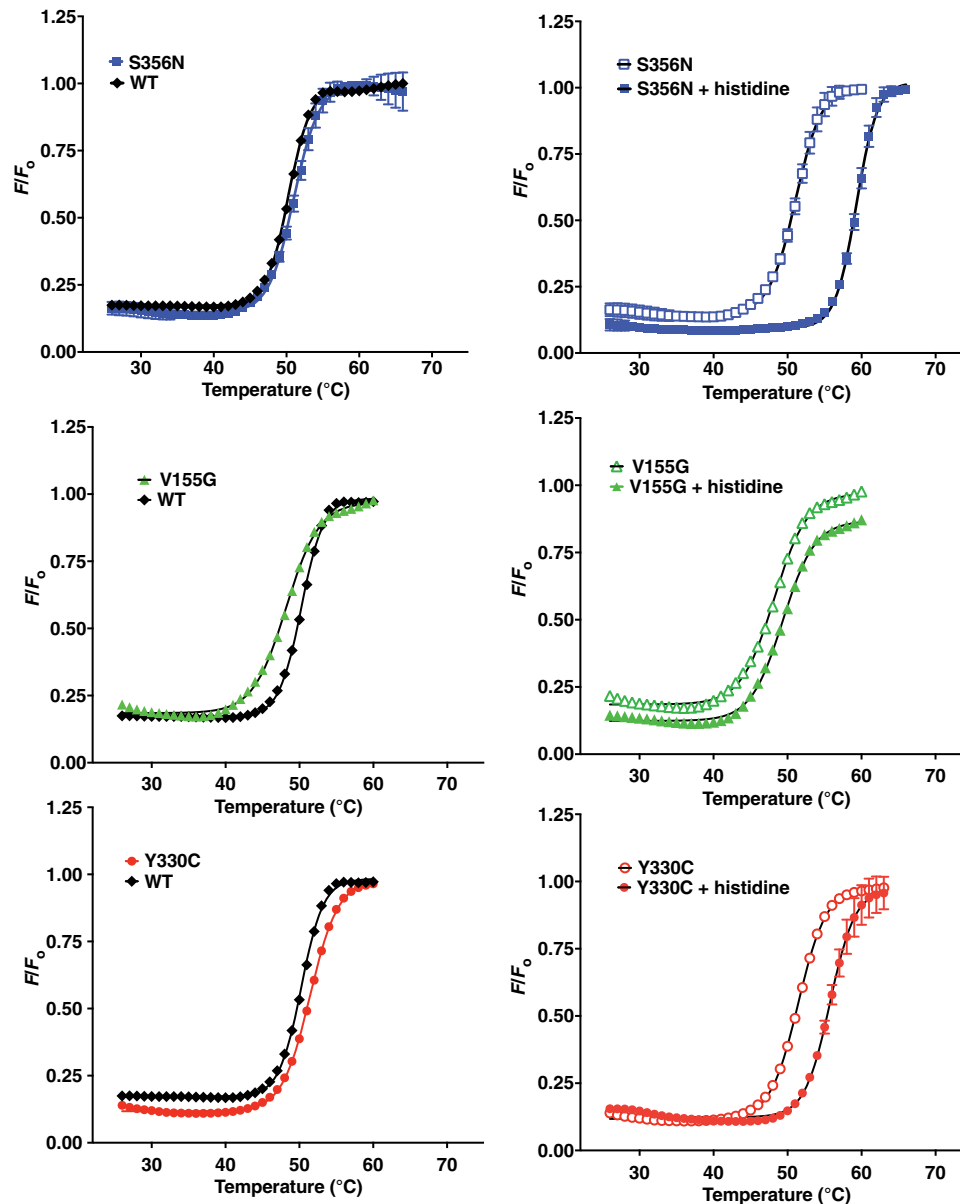


FIGURE 8 Differential scanning fluorimetry of neuropathy-associated HARS enzymes and their interactions with substrates. **A–C**: Melting temperature of apo wild-type or mutant HARS enzymes determined at a concentration of 10 mM WT enzyme (black diamonds, \blacklozenge); p.Ser356Asn HARS (blue squares, \blacksquare); p.Val155Gly (green triangles, \blacklozenge); and p.Tyr330Cys HARS (red circles, \bullet). **D–F**: Stabilization by histidine was investigated by incubation of mutant HARS enzymes with 5 mM histidine. Empty symbols represent apo enzymes, while filled symbols represent histidine bound complexes of p.Ser356Asn HARS (**D**); p.Val155Gly HARS (**E**); and p.Tyr330Cys HARS (**F**). Thermal shift curves are representations of neuropathy-associated mutants measured in duplicate

weaker tertiary interactions and thus reduced dimer stability (Nangle, Zhang, Xie, Yang, & Schimmel, 2007). Given the location of the HARS mutants in the active site, we considered the possibility that the decreased activity of these mutants might be a consequence of reduced dimer stability. To address this hypothesis, we subjected highly purified preparations of each of the mutant proteins and a WT control to sedimentation velocity experiments at various loading concentrations. In these experiments, we monitored protein absorbance at 230 nm, allowing the experiments to be performed at concentrations that would be in the range of the equilibrium dissociation constant (K_d) for the dimer. As shown in Supp. Figure S1, the molar mass distributions of the WT and mutant proteins were closely similar. For each

mutant, a major species was observed that had a molar mass that was in excellent agreement with the dimer form of HARS (Table 4 and Supp. Figure S1). In none of the mutants was there a detectable amount of material corresponding to the monomeric form of the enzyme. On the basis of these results, we conclude that the pathophysiology of these mutants is unlikely to be the result of a weakened dimeric interface.

4 | DISCUSSION

Mutations in five ARS genes were previously implicated in CMT disease (Jordanova et al., 2006; Latour et al., 2010; Safka Brozkova et al.,

2015; Storkebaum, 2016; Tsai et al., 2017; Vester et al., 2013). A central question emerging from those studies is the degree to which the CMT disease is a direct consequence of a loss of canonical ARS function, or is instead linked to one or more potential secondary functions. In this article, we describe detailed functional analyses of three *HARS* mutations linked to CMT. The characterization of these mutants showed that they all displayed losses in catalytic activity when assessed in vivo and in vitro. Notably, the extent of decrease in catalytic activity correlated with the loss of ability to support yeast growth. The most active of the three mutants (p.Val155Gly *HARS*) was the only one of the three mutants that retained some ability to support yeast growth when studied in the human *HARS* open-reading frame. In contrast to previous work analyzing ARS mutants linked to CMT, each mutant was fully characterized with respect to defects associated with recognition of each substrate; indeed, biochemical analysis of CMT-associated *HARS* mutations has not been previously reported. The novel finding emerging from our analysis is that all three mutants displayed substantially elevated Michaelis constants for ATP, and two of the three (p.Tyr330Cys and p.Val155Gly) displayed an elevated K_M for histidine. Notably, none of the three exhibited an altered K_M for tRNA. Collectively, these mutants represent some of the best-characterized examples of ARSs where specific defects in substrate recognition that produce reduced aminoacylation function are specifically linked to CMT. It would therefore be valuable to know if other CMT-associated ARS mutations lead to similar alterations in substrate interactions, as such information would help develop comprehensive models to explain the gene-disease relationships.

4.1 | Strength of the evidence implicating the newly identified *HARS* mutations in neuropathy

Implicating ARS mutations in peripheral neuropathy requires data showing that the variants segregate with disease in large pedigrees and are absent at high frequencies in the general population. Indeed, the majority of previously implicated ARS mutations meet these criteria (Oprescu et al., 2017). When genetic data are impossible to obtain, functional studies can be employed to predict pathogenicity, provided that the functional assays are informative. With respect to ARS mutations, enzyme kinetic and yeast complementation assays are informative for predicting mutational pathogenicity (Oprescu et al., 2017). Several independent lines of evidence allow us to conclude that p.Val155Gly and p.Tyr330Cys *HARS* are the causal mutations in Family 1 and Family 2, respectively. Notably, the mutations segregate with the CMT phenotype in pedigrees (albeit in a small family for

p.Tyr330Cys), occur at highly conserved amino acids, are absent from variant databases, and result in loss-of-function effects similar to other CMT-associated ARS variants. By contrast, the evidence for the role of p.Ser356Asn in the CMT phenotype in Family 3 is less convincing. Specifically, the patient's unaffected mother is heterozygous for p.Ser356Asn *HARS*, and this variant is present (albeit at a very low frequency) in the gnomAD variant database. However, the fact that p.Ser356Asn affects a highly conserved amino-acid residue and displays impaired function similar to validated, disease-associated ARS mutations strongly supports the conclusion that it may be a pathogenic variant (Safka Brozkova et al., 2015; Vester et al., 2013). One possibility is that p.Ser356Asn *HARS* has reduced penetrance similar to certain *GARS* mutations (Sivakumar et al., 2005). This proposal is supported by the low frequency of validated, CMT-associated ARS mutations in the gnomAD variant database (e.g., p.Gly240Arg *GARS*; <https://gnomad.broadinstitute.org/variant/7-30649345-G-C>; Gly240Arg is equivalent to p.Gly294Arg on a longer protein isoform). Conversely, it is possible that p.Ser356Asn is not the disease-causing mutation in Family 3 despite the deleterious effect on enzyme function. Thus, we conclude that p.Ser356Asn *HARS* is an excellent candidate for pathogenicity in Family 3, but that further genetic and phenotypic evidence is required to implicate this variant in CMT disease.

4.2 | Structural justification for activity defects

All three of the amino-acid substitutions analyzed here alter amino acids located in the catalytic domain, consistent with their pronounced effect on aminoacylation. Visualization of these substitutions in the context of available X-ray structure of human *HARS* provides insights into potential structural and functional consequences. While Ser356 does not appear to be involved directly in substrate binding interactions, it may be important for positioning other amino-acid residues within the active site that are critical for binding of the ATP substrate. ATP binding in the active site of *HARS* is dependent on magnesium ions that are coordinated to the non-bridging oxygens of the β and γ phosphates of ATP, and the strictly conserved glutamate in Motif 2. In the human *HARS* histidine complex (no ATP), Ser356 is within 2.5 Å of Arg 388 (Figure 2A), the conserved motif 3 arginine that (based on the *E. coli* complex) is predicted to interact with the gamma phosphate of ATP (Figure 2B). Important caveats regarding the likely effects of p.Ser356Asn are that, firstly, a complex with ATP is not available, and secondly, that much of the loop between strands B9 and B10 in which Ser356 residue resides is disordered in the various human *HARS*

TABLE 4 PCSA–Monte Carlo results (straight-line parameterization) from sedimentation velocity experiment

Species	Molar mass (kDa)	$D (\times 10^{-7} \text{ cm}^2/\text{sec}^2)$	$s (\times 10^{-13} \text{ sec})$	f/f_0	RMSD
WT	118.5 (111.6, 125.5)	4.54 (4.43, 4.66)	5.67 (5.48, 5.85)	1.44 (1.43, 1.45)	0.0025
p.Val155Gly	122.0 (110.6, 133.5)	4.43 (4.20, 4.65)	5.68 (5.42, 5.94)	1.46 (1.44, 1.49)	0.0032
p.Tyr330Cys	120.6 (116.3, 124.9)	4.52 (4.50, 4.55)	5.74 (5.51, 5.97)	1.44 (1.42, 1.46)	0.0028
p.Ser356Asn	120.0 (110.3, 129.6)	4.41 (4.34, 4.49)	5.57 (5.21, 5.93)	1.48 (1.46, 1.49)	0.0034

Values in parenthesis are 95% confidence intervals from the Monte Carlo analysis. The theoretical molar mass of *HARS* WT dimer is 114.9 kDa, indicating the observed species is a dimer. The residual mean square deviation (RMSD) of the fit is shown in units of absorbance at 230 nm.

structures, and has different conformations in the different subunits of the asymmetric unit (Koh et al., 2014). Hence, it is difficult to make definitive conclusions about the potential role of Ser356 in stabilizing interactions in the bound complex, and about the consequences of substitution with asparagine. In any event, the elevated K_M for ATP seen with p.Ser356Asn could be seen as a likely outcome of a local disruption of contacts to the gamma phosphate.

The one mutant that would be predicted to have the most severe consequence for HARS function is p.Tyr330Cys, which substitutes a highly conserved tyrosine in the His A motif that constitutes part of the binding site for histidine (Figure 5). Notably, this residue has different conformations in the apo versus histidine bound human cytoplasmic HARS complex. In the apo complex without substrates (4×50), Y330 adopts a conformation directed away from the active site, pointing toward solvent and donating a hydrogen bond to the main chain carbonyl of Gly108 (Figure 2C). In the complex of HARS with its amino acid substrate, Y330 moves some 8 Å to approach within 3.1 of the alpha-carbon of histidine (Figure 2D). In this bound conformation, Y330 may further stabilize the histidine binding pocket by engaging in a stacking interaction with the polar group of the neighboring tyrosine in position 331.

A similar effect may underlie the effect of p.Val155Gly on HARS function. Notably, this mutant exhibited a lower melting temperature than the other mutants, but the substitution had no effect on the association constant for the dimer. Analysis of the human HARS–histidine complex and comparison to the *E. coli* HisRS–histidinol ATP complex suggests that p.Val155Gly is unlikely to substitute a residue that interacts directly with ATP (Figure 2E). However, Val155 is in the region of the active site near where ATP binds, and the valine can potentially make a CH- π interaction with the neighboring hydrophobic Phe171 in the active site (Figure 2E). Phe171 in human HARS corresponds to Phe125 in the *E. coli* enzyme (Arnez et al., 1995), which makes a critical stacking interaction with the adenine ring (Figure 2F). The substitution of glycine for valine at position 155 may allow greater conformational flexibility on the part of Phe171, reducing its ability to generate stable binding pocket for ATP. The effects of this disruption are apparent in the elevated K_M value for ATP observed for p.Val155Gly. Additionally, a glycine substitution would permit greater conformational freedom in the accessible phi-psi angles within the peptide backbone of the beta sheet, potentially accounting for the lower melting temperature in the absence of substrate. Furthermore, a less constrained beta sheet created by the glycine substitution could directly impact the helix 3, which contains the “TXE” motif for histidine binding. This provides a structural rationale for the decreased T_m of the p.Val155Gly apo enzyme, the dramatically reduced T_m in the presence of histidine (Table 3), and the elevated K_M for histidine (Table 2).

4.3 | The vast majority of ARS mutations impair enzyme activity

Previous studies examining the links between mutations in ARS genes and CMT have addressed the question of whether mutations lead to a significant loss of aminoacylation activity, or a change in an as yet undetermined secondary function. The biochemical analyses in this study

indicate that CMT-linked HARS mutations confer significant reductions in aminoacylation function, in accordance with what has been described for AARS mutations (McLaughlin, et al., 2012). These AARS mutations, like the described HARS mutations, also fail to complement yeast growth over a background where the endogenous yeast gene has been disrupted (Oprescu et al., 2017). Thus, for AARS and HARS mutations, the link to CMT appears to be directly associated with a loss of aminoacylation function.

The link between CMT and reduced ARS function is slightly less clear for two other ARS genes, GARS and YARS. In these cases, multiple mutations are linked to the disease, some of which have clear reductions in aminoacylation, and some of which appear to retain significant activity. In GARS, 12 GARS mutations have been associated with CMT disease, the majority of which are deleterious to enzyme function (Oprescu et al., 2017). In the case of YARS, two mutants are reported to have significantly reduced activity (Jordanova et al., 2006) but one (p.Glu196Lys) appears to be much more active, or even unaffected (Froelich & First, 2011). However, the p.Glu196Lys mutant and another CMT-associated mutation at the same codon (p.Glu196Gln) were unable to fully support yeast cell growth in complementation studies (Gonzaga-Jauregui et al., 2015; Jordanova et al., 2006). Furthermore, studies employing a *D. melanogaster* model of CMT show that, despite its near WT activity in vitro, p.Glu196Lys YARS leads to decreased protein synthesis rates in flies (Niehues et al., 2015). These and other results suggest that, in the context of specialized cell types, the consequences of a particular human pathogenic ARS mutation may be difficult to predict a priori. Mutations that lead to decreased activity may have limited phenotypic impact owing to the fact that, under normal conditions, protein synthesis can be met by less than 100% activity of a given tRNA synthetase. Conversely, a mutation that has limited impact on aminoacylation in vitro may exert more deleterious impact in vivo, owing to folding defects that promote proteotoxic stress. Discrepancies may arise as a consequence of additional interactions with other proteins and/or RNAs that are necessary to execute all phases of protein synthesis. Moving forward, a critical question to be addressed for each CMT-related ARS allele is if protein synthesis is affected as a direct downstream consequence of impaired aminoacylation.

4.4 | Proposed gain-of-function effects of ARS mutations

Clearly more research is needed to resolve the effect of CMT-associated ARS mutations on enzyme function. As an alternative to loss-of-function mechanisms, multiple gain-of-function hypotheses have been proposed, specifically for GARS mutations (Motley, Talbot, & Fischbeck, 2010). For example, a mechanism in which mutant monomeric GARS binds to the VEGF receptor neuropilin-1 and alters neuronal signaling has been proposed in the context of a mouse model (He et al., 2015). As yet, the relevance of this model to human disease-associated mutations is not fully clear. However, three human mutant GARS proteins (p.Glu71Gly, p.Leu129Pro, and p.Gly240Arg) were shown to bind to neuropilin-1 in vitro. Additionally, it was argued that the propensity of mutant GARS to bind to neuropilin-1 was linked to weakened dimer formation (Xie, Nangle, Zhang, Schimmel, & Yang,

2007). While the findings reported here do not explicitly address the neuropilin-1 hypothesis, our characterization of HARS mutant proteins indicates that, despite a loss of canonical catalytic function, there is no evidence for weakened dimerization (Supp. Figure S1). It should also be noted that, despite the linkage of over 80 loci to CMT disease, neither mutations in neuropilin-1 nor in any of the ligands for this receptor have been identified in patients with CMT disease.

5 | CONCLUSIONS

Here, we present data that for the first time link impaired enzyme activity to HARS-associated peripheral neuropathy. This observation dictates considerations of how altered tRNA charging might affect peripheral nerve function. Human peripheral nerve axons can extend more than a meter in length, and transport of essential proteins to the cell periphery is essential for maintaining axon function (Giuditta, Dettbarn, & Brzin, 1968). There is increasing evidence of local protein translation along axons and at synapses, but the role of ARSs in this process is still not well understood (Holt & Schuman, 2013). Moving forward, it will be important to directly test if CMT-associated ARS mutations alter specific aspects of protein translation. In summary, additional studies are required to determine if CMT-associated ARS mutations act via a loss-of-function or gain-of-function mechanism; we suggest that these two mechanisms are not mutually exclusive. Our study presents data that further supports a loss-of-function molecular pathology and provides key data, newly applied methods, and novel reagents for studying the pathological mechanism of ARS-associated human disease.

ACKNOWLEDGMENTS

We are grateful to the patients and their families who participated in this study.

DISCLOSURE STATEMENT

The authors declare no conflict of interest.

ORCID

Anthony Antonellis  <http://orcid.org/0000-0002-5820-3156>

Christopher Francklyn  <http://orcid.org/0000-0002-6075-4037>

REFERENCES

- Abbott, J. A., Francklyn, C. S., & Robey-Bond, S. M. (2014). Transfer RNA and human disease. *Frontiers in Genetics*, 5, Article 158, 1–18.
- Abbott, J. A., Guth, E., Kim, C., Regan, C., Siu, V. M., Rugar, C. A., ... Robey-Bond, S. M. (2017). The Usher Syndrome type IIIB histidyl-tRNA synthetase mutation confers temperature sensitivity. *Biochemistry*, 56, 3619–3631.
- Antonellis, A., Ellsworth, R. E., Sambuughin, N., Puls, I., Abel, A., Lee-Lin, S. Q., ... Middleton, L. T. and others (2003). Glycyl tRNA synthetase mutations in Charcot-Marie-Tooth disease type 2D and distal spinal muscular atrophy type V. *American Journal of Human Genetics*, 72(5), 1293–1299.
- Antonellis, A., & Green, E. D. (2008). The role of aminoacyl-tRNA synthetases in genetic diseases. *Annual Review of Genomics and Human Genetics*, 9, 87–107.
- Arnez, J. G., Harris, D. C., Mitschler, A., Rees, B., Francklyn, C. S., & Moras, D. (1995). Crystal structure of histidyl-tRNA synthetase from *Escherichia coli* complexed with histidyl-adenylate. *EMBO Journal*, 14(17), 4143–4155.
- Bird, T. D. (1993). Charcot-Marie-Tooth hereditary neuropathy overview. In Adam, M. P., Ardinger, H. H., Pagon, R. A., Wallace, S. E., Bean, L. J. H., Mefford, H. C., ... Ledbetter, N., (editors). *GeneReviews(R)*. Seattle, WA: University of Washington.
- Boeke, J. D., LaCrute, F., & Fink, G. R. (1984). A positive selection for mutants lacking orotidine-5'-phosphate decarboxylase activity in yeast: 5-fluoro-orotic acid resistance. *Molecular and General Genetics*, 197(2), 345–346.
- Brookes, E., Cao, W., & Demeler, B. (2010). A two-dimensional spectrum analysis for sedimentation velocity experiments of mixtures with heterogeneity in molecular weight and shape. *European Biophysics Journal*, 39(3), 405–414.
- Brookes, E. D. B. (2006). Analytical ultracentrifugation data analysis with UltraScan-III. Analytical ultracentrifugation: Instrumentation, software, and applications. In C.C.H. Wandrey (Ed.), *Analytical ultracentrifugation VIII. Progress in colloid and polymer science*. Berlin, Heidelberg: Springer.
- Brookes, E. H., & Demeler, B. (2008). Parallel computational techniques for the analysis of sedimentation velocity experiments in UltraScan. *Colloid and Polymer Science*, 286(2), 139–148.
- Burns, J., Ouvrier, R., Estilow, T., Shy, R., Laura, M., Pallant, J. F., ... Finkel, R. S. (2012). Validation of the Charcot-Marie-Tooth disease pediatric scale as an outcome measure of disability. *Annals of Neurology*, 71(5), 642–652.
- De Lorenzo, F., Straus, D. S., & Ames, B. N. (1972). Histidine regulation in *Salmonella typhimurium*. X. Kinetic studies of mutant histidyl transfer ribonucleic acid synthetases. *Journal of Biological Chemistry*, 247(8), 2302–2307.
- Demeler, B. (2010). Methods for the design and analysis of sedimentation velocity and sedimentation equilibrium experiments with proteins. *Current Protocols in Protein Science*, Chapter 7:UNit 7, 13, 7.13.1–7.13.24.
- Demeler, B., & Brookes, E. (2008). Monte Carlo analysis of sedimentation experiments. *Colloid and Polymer Science*, 286(2), 129–137.
- Demeler, B., Gorbet, G., Zollars, D., Dubbs, B., Brookes, E., & Cao, W. (2016). UltraScan-III version 3.5: A comprehensive data analysis software package for analytical ultracentrifugation experiments. Retrieved from <https://www.ultrascan3.uthscsa.edu/>
- Dyck, P. J., & Lambert, E. H. (1968). Lower motor and primary sensory neuron diseases with peroneal muscular atrophy. II. Neurologic, genetic, and electrophysiologic findings in various neuronal degenerations. *Archives of Neurology*, 18(6), 619–625.
- Fahoum, S. K., & Yang, D. C. (1987). Purification of mammalian histidyl-tRNA synthetase and its interaction with myositis-specific anti-Jo-1 antibodies. *Biochemistry*, 26(18), 5871–5877.
- Froelich, C. A., & First, E. A. (2011). Dominant Intermediate Charcot-Marie-Tooth disorder is not due to a catalytic defect in tyrosyl-tRNA synthetase. *Biochemistry*, 50(33), 7132–7145.
- Frohlich, D., Suchowerska, A. K., Spencer, Z. H., von Jonquieres, G., Klugmann, C. B., Bongers, A., ... Klugmann, M. (2017). In vivo characterization of the aspartyl-tRNA synthetase DARS: Homing in on the leukodystrophy HBSL. *Neurobiology of Disease*, 97(Pt A), 24–35.
- Giuditta, A., Dettbarn, W. D., & Brzin, M. (1968). Protein synthesis in the isolated giant axon of the squid. *Proceedings of the National Academy of Sciences of the United States of America*, 59(4), 1284–1287.

- Gonzaga-Jauregui, C., Harel, T., Gambin, T., Kousi, M., Griffin, L. B., Francescato, L., ... Lupski, J. R. (2015). Exome sequence analysis suggests that genetic burden contributes to phenotypic variability and complex neuropathy. *Cell Reports*, 12(7), 1169–1183.
- Gonzalez, M., Falk, M. J., Gai, X., Postrel, R., Schule, R., & Zuchner, S. (2015). Innovative genomic collaboration using the GENESIS (GEM.app) platform. *Human Mutation*, 36(10), 950–956.
- Gonzalez, M., McLaughlin, H., Houlden, H., Guo, M., Yo-Tsen, L., Hadjivassiliou, M., ... Reilly, M. M. and others (2013). Exome sequencing identifies a significant variant in methionyl-tRNA synthetase (MARS) in a family with late-onset CMT2. *Journal of Neurology, Neurosurgery, and Psychiatry*, 84(11), 1247–1249.
- Gorbet, G., Devlin, T., Hernandez Uribe, B. I., Demeler, A. K., Lindsey, Z. L., Ganji, S., ... Demeler, B. (2014). A parametrically constrained optimization method for fitting sedimentation velocity experiments. *Biophysical Journal*, 106(8), 1741–1750.
- He, W., Bai, G., Zhou, H., Wei, N., White, N. M., Lauer, J., ... Yang, X. L. (2015). CMT2D neuropathy is linked to the neomorphic binding activity of glycyl-tRNA synthetase. *Nature*, 526(7575), 710–714.
- Hirano, M., Oka, N., Hashiguchi, A., Ueno, S., Sakamoto, H., Takashima, H., ... Nakamura, Y. (2016). Histopathological features of a patient with Charcot-Marie-Tooth disease type 2U/AD-CMTax-MARS. *Journal of the Peripheral Nervous System*, 21(4), 370–374.
- Holt, C. E., & Schuman, E. M. (2013). The central dogma decentralized: New perspectives on RNA function and local translation in neurons. *Neuron*, 80(3), 648–657.
- Hyun, Y. S., Park, H. J., Heo, S. H., Yoon, B. R., Nam, S. H., Kim, S. B., ... Chung, K. W. (2014). Rare variants in methionyl- and tyrosyl-tRNA synthetase genes in late-onset autosomal dominant Charcot-Marie-Tooth neuropathy. *Clinical Genetics*, 86(6), 592–594.
- Ibba, M., & Soll, D. (2000). Aminoacyl-tRNA synthesis. *Annual Review of Biochemistry*, 69, 617–650.
- Jerath, N. U., & Shy, M. E. (2015). Hereditary motor and sensory neuropathies: Understanding molecular pathogenesis could lead to future treatment strategies. *Biochimica Et Biophysica Acta*, 1852(4), 667–678.
- Jordanova, A., Irobi, J., Thomas, F. P., Van Dijck, P., Meerschaert, K., Dewil, M., ... Timmerman, V. (2006). Disrupted function and axonal distribution of mutant tyrosyl-tRNA synthetase in dominant intermediate Charcot-Marie-Tooth neuropathy. *Nature Genetics*, 38(2), 197–202.
- Koh, C. Y., Kim, J. E., Wetzell, A. B., de van der Schueren, W. J., Shibata, S., Ranade, R. M., ... Hol, W. G. (2014). Structures of Trypanosoma brucei methionyl-tRNA synthetase with urea-based inhibitors provide guidance for drug design against sleeping sickness. *PLoS Neglected Tropical Diseases*, 8(4), e2775, 1–13.
- Larkin, M. A., Blackshields, G., Brown, N. P., Chenna, R., McGettigan, P. A., McWilliam, H., ... Higgins, D. G. (2007). Clustal W and Clustal X version 2.0. *Bioinformatics*, 3(21), 2947–2948.
- Latour, P., Thauvin-Robinet, C., Baudelet-Mery, C., Soichot, P., Cusin, V., Faivre, L., ... Rousson, R. (2010). A major determinant for binding and aminoacylation of tRNA(Ala) in cytoplasmic Alanyl-tRNA synthetase is mutated in dominant axonal Charcot-Marie-Tooth disease. *American Journal of Human Genetics*, 86(1), 77–82.
- Laue, T. M., Shah, B. D., Ridgeway, T. M., & Pelletier, S. L. (1992). In S. Harding, A. Rowe (Eds.), *Analytical ultracentrifugation in biochemistry and polymer science* (pp. 90–125). Royal Society of Chemistry, Cambridge, UK.
- Lee, Y. H., Chang, C. P., Cheng, Y. J., Kuo, Y. Y., Lin, Y. S., & Wang, C. C. (2017). Evolutionary gain of highly divergent tRNA specificities by two isoforms of human histidyl-tRNA synthetase. *Cellular and Molecular Life Sciences*, 74(14), 2663–2677.
- Lek, M., Karczewski, K. J., Minikel, E. V., Samocha, K. E., Banks, E., Fennell, T., ... Cummings, B. B. and others (2016). Analysis of protein-coding genetic variation in 60,706 humans. *Nature*, 536(7616), 285–291.
- Lupo, V., Garcia-Garcia, F., Sancho, P., Tello, C., Garcia-Romero, M., Villarreal, L., ... Espinós, C. (2016). Assessment of targeted next-generation sequencing as a tool for the diagnosis of Charcot-Marie-Tooth disease and hereditary motor neuropathy. *The Journal of Molecular Diagnostics*, 18(2), 225–234.
- McLaughlin, H. M., Sakaguchi, R., Giblin, W., NISC Comparative Sequencing Program, Wilson, T. E., Biesecker, L., ... Antonellis, A. (2012). A recurrent loss-of-function alanyl-tRNA synthetase (AARS) mutation in patients with Charcot-Marie-Tooth disease type 2N (CMT2N). *Human Mutation*, 33(1), 244–253.
- Meyer-Schuman, R., & Antonellis, A. (2017). Emerging mechanisms of aminoacyl-tRNA synthetase mutations in recessive and dominant human disease. *Human Molecular Genetics*, 26, R114–R127.
- Motley, W. W., Talbot, K., & Fischbeck, K. H. (2010). GARS axonopathy: Not every neuron's cup of tRNA. *Trends in Neuroscience*, 33(2), 59–66.
- Nam, S. H., Hong, Y. B., Hyun, Y. S., Nam da, E., Kwak, G., Hwang, S. H., ... Chung, K. W. (2016). Identification of genetic causes of inherited peripheral neuropathies by targeted gene panel sequencing. *Molecules and Cells*, 39(5), 382–388.
- Nangle, L. A., Zhang, W., Xie, W., Yang, X. L., & Schimmel, P. (2007). Charcot-Marie-Tooth disease-associated mutant tRNA synthetases linked to altered dimer interface and neurite distribution defect. *Proceedings of the National Academy of Sciences of the United States of America*, 104(27), 11239–11244.
- Niehues, S., Bussmann, J., Steffes, G., Erdmann, I., Kohrer, C., Sun, L., ... Storkebaum, E. (2015). Impaired protein translation in Drosophila models for Charcot-Marie-Tooth neuropathy caused by mutant tRNA synthetases. *Nature Communications*, 6, 7520, 1–12.
- Niesen, F. H., Berglund, H., & Vedadi, M. (2007). The use of differential scanning fluorimetry to detect ligand interactions that promote protein stability. *Nature Protocols*, 2(9), 2212–2221.
- Oprescu, S. N., Griffin, L. B., Beg, A. A., & Antonellis, A. (2017). Predicting the pathogenicity of aminoacyl-tRNA synthetase mutations. *Methods*, 113, 139–151.
- Pareyson, D., & Marchesi, C. (2009a). Diagnosis, natural history, and management of Charcot-Marie-Tooth disease. *Lancet Neurology*, 8(7), 654–667.
- Pareyson, D., & Marchesi, C. (2009b). Natural history and treatment of peripheral inherited neuropathies. *Advances in Experimental Medicine and Biology*, 652, 207–224.
- Pareyson, D., Marchesi, C., & Salsano, E. (2009). Hereditary predominantly motor neuropathies. *Current Opinion in Neurology*, 22(5), 451–459.
- Pierce, S. B., Chisholm, K. M., Lynch, E. D., Lee, M. K., Walsh, T., Opitz, J. M., ... King, M. C. (2011). Mutations in mitochondrial histidyl tRNA synthetase HARS2 cause ovarian dysgenesis and sensorineural hearing loss of Perault syndrome. *Proceedings of the National Academy of Sciences of the United States of America*, 108(16), 6543–6548.
- Puffenberger, E. G., Jinks, R. N., Sougnez, C., Cibulskis, K., Willert, R. A., Achilly, N. P., ... Strauss, K. A. (2012). Genetic mapping and exome sequencing identify variants associated with five novel diseases. *Plos One*, 7(1), e28936, 1–15.
- Robert, X., & Gouet, P. (2014). Deciphering key features in protein structures with the new ENDscript server. *Nucleic Acids Research*, 42(Web Server issue), W320–W324.
- Safka Brozkova, D., Deconinck, T., Griffin, L. B., Ferbert, A., Haberlova, J., Mazanec, R., ... Baets, J. (2015). Loss of function mutations in HARS cause a spectrum of inherited peripheral neuropathies. *Brain*, 138(Pt 8), 2161–2172.

- Schuck, P. (1999). Sedimentation equilibrium analysis of interference optical data by systematic noise decomposition. *Analytical Biochemistry*, 272(2), 199–208.
- Shy, M. E., Blake, J., Krajewski, K., Fuerst, D. R., Laura, M., Hahn, A. F., ... Reilly, M. (2005). Reliability and validity of the CMT neuropathy score as a measure of disability. *Neurology*, 64(7), 1209–1214.
- Simons, C., Griffin, L. B., Helman, G., Golas, G., Pizzino, A., Bloom, M., ... Vanderver, A. (2015). Loss-of-function alanyl-tRNA synthetase mutations cause an autosomal-recessive early-onset epileptic encephalopathy with persistent myelination defect. *American Journal of Human Genetics*, 96(4), 675–681.
- Sivakumar, K., Kyriakides, T., Puls, I., Nicholson, G. A., Funalot, B., Antonellis, A., ... Goldfarb, L. G. (2005). Phenotypic spectrum of disorders associated with glycyI-tRNA synthetase mutations. *Brain*, 128(Pt 10), 2304–2314.
- Skre, H. (1974). Genetic and clinical aspects of Charcot-Marie-Tooth's disease. *Clinical Genetics*, 6(2), 98–118.
- Storkebaum, E. (2016). Peripheral neuropathy via mutant tRNA synthetases: Inhibition of protein translation provides a possible explanation. *Bioessays*, 38(9), 818–829.
- Stum, M., McLaughlin, H. M., Kleinbrink, E. L., Miers, K. E., Ackerman, S. L., Seburn, K. L., ... Burgess, R. W. (2011). An assessment of mechanisms underlying peripheral axonal degeneration caused by aminoacyl-tRNA synthetase mutations. *Molecular and Cellular Neuroscience*, 46(2), 432–443.
- Timmerman, V., Strickland, A. V., & Zuchner, S. (2014). Genetics of Charcot-Marie-Tooth (CMT) disease within the frame of the human genome project success. *Genes*, 5(1), 13–32.
- Tsai, P. C., Soong, B. W., Mademan, I., Huang, Y. H., Liu, C. R., Hsiao, C. T., ... Lee, Y. C. (2017). A recurrent WARS mutation is a novel cause of autosomal dominant distal hereditary motor neuropathy. *Brain*, 140, 1252–1266.
- Vester, A., Velez-Ruiz, G., McLaughlin, H. M., Lupski, J. R., Talbot, K., Vance, J. M., ... Antonellis, A. (2013). A loss-of-function variant in the human histidyl-tRNA synthetase (HARS) gene is neurotoxic in vivo. *Human Mutation*, 34(1), 191–199.
- Wolfson, A. D., Pleiss, J. A., & Uhlenbeck, O. C. (1998). A new assay for tRNA aminoacylation kinetics. *RNA*, 4(8), 1019–1023.
- Xie, W., Nangle, L. A., Zhang, W., Schimmel, P., & Yang, X. L. (2007). Long-range structural effects of a Charcot-Marie-Tooth disease-causing mutation in human glycyI-tRNA synthetase. *Proceedings of the National Academy of Sciences of the United States of America*, 104(24), 9976–9981.
- Zhang, X., Ling, J., Barcia, G., Jing, L., Wu, J., Barry, B. J., ... Weimer, J. M. (2014). Stein Q and others Mutations in QARS, encoding glutaminyl-tRNA synthetase, cause progressive microcephaly, cerebral-cerebellar atrophy, and intractable seizures. *American Journal of Human Genetics*, 94(4), 547–558.

SUPPORTING INFORMATION

Additional Supporting Information may be found online in the supporting information tab for this article.

How to cite this article: Abbott JA, Meyer-Schuman R, Lupo V, et al. Substrate interaction defects in histidyl-tRNA synthetase linked to dominant axonal peripheral neuropathy. *Human Mutation*. 2018;39:415–432. <https://doi.org/10.1002/humu.23380>